The Dilated Cardiomyopathy-Associated *MYH7* Mutation R369Q Displays Different Phenotypes Across a Multiscale Study of Contraction

Aditi M. Prabhala

A thesis

submitted in partial fulfillment of the

requirements for the degree of

Master of Science

University of Washington

2025

Committee:

Michael Regnier

Farid Moussavi-Harami

Program Authorized to Offer Degree:

Bioengineering

University of Washington

Abstract

The Dilated Cardiomyopathy-Associated *MYH7* Mutation R369Q Displays Different Phenotypes Across a Multiscale Study of Contraction

Aditi M. Prabhala

Chair of the Supervisory Committee:

Michael Regnier

Bioengineering

Heart failure is a debilitating condition whose mortality rate is currently increasing. Dilated cardiomyopathy (DCM) is one major contributor to heart failure cases, yet little is known about the pathogenesis of the disease and medications only serve to manage symptoms. Many cases of DCM are genetically associated with pathogenic variants of the sarcomeric proteins which make up the contractile machinery of cardiomyocytes, the contractile cells of the heart. Here, we present a multiscale study of the DCM-associated likely pathogenic β-myosin heavy chain variant R369Q, which is thought to impede contractility through alteration of thin filament interactions. Beginning from the tissue level, we demonstrate that engineered heart tissues recapitulate the DCM phenotype but that suggested results are not necessarily consistent on smaller levels such as the cell. Only by probing several scales of contraction from the tissue down to the molecule were we

able to propose a nuanced mechanism of disease pathogenesis that aligned with our various experimental models. Thus, we suggest that a multiscale approach is powerful and necessary to understand the mechanisms of disease progression and must serve as the foundation for development of novel therapeutics for heart failure and DCM.

Acknowledgements

I would not have been able to complete this work without the support of all the members of the Regnier Lab. Particularly, I would like to thank Dr. Mike Regnier for his constant support and for pushing me to pursue a challenging research project as an undergraduate. I would also like to thank my primary mentors, Kerry Kao and Dr. Matt Childers, whose guidance and mentorship has been invaluable to me over the years. I would also like to acknowledge our collaboration with Dr. Bill Lehman's lab at Boston University. Their work on the R369Q mutation has opened up new avenues for my own studies and made me excited to keep pursuing this project. Gratefully, I acknowledge all members of the Regnier and Moussavi-Harami labs for being incredibly supportive and kind throughout my research journey…no matter what anyone has going on in their own experiments, my colleagues are always open to sharing tips for running experiments, funny jokes, and sage advice. This work wouldn't be possible without them.

I would also like to thank my friends. As an extremely social person, I would not be able to survive without the video calls, late-night study sessions, catch-up lunches, and existential conversations. You all are the reason that I will forever look back at this stage of life fondly. Your love and support keep me afloat and energized to pursue my goals.

Finally, and most importantly, I would like to thank my family. To my parents, who have worked hard and sacrificed for our family and always made me believe I could do anything, your love and compassion has meant everything. To my sisters, thank you for being my best friends and keeping my spirits up through your humor and love. I would not be who I am today without you.

For Amma and Nanna

You always inspire me to be the best version of myself.

Table of Contents

LIST OF FIGURES

Chapter 1

Motivations and Current State of the Field

1.1 Dilated cardiomyopathy poses a significant healthcare burden

1.1.1 Dilated cardiomyopathy and heart failure

Heart failure (HF) is defined as a condition in which the heart cannot pump blood effectively enough to meet the body's needs and impacts over 56 million people worldwide (1). The condition can be incredibly debilitating in day-to-day life with symptoms such as reduced exercise tolerance, fatigue, peripheral edema, and breathlessness as well as mental burden akin to other chronic diseases like cancer (1,2). In addition to this human burden, the costs of HF are expected to rise to almost $70 billion by 2030 in the United States alone, indicating a clinical and economic reason to better understand and treat cardiovascular conditions with the potential to progress to heart failure (3).

One key contributor to heart failure is dilated cardiomyopathy (DCM). In fact, DCM is the second leading cause of heart failure, accounting for approximately 36% of cases, as well as the most common indication for a heart transplant (4,5). The staggering degree of DCM's contribution to heart failure, as well as DCM's own dismal 5-year survival rate of 50%, demonstrates the need to better understand this pathology and design treatments to prevent the progression to end-stage heart failure (6).

1.1.2 Genetics frequently underpin dilated cardiomyopathy

Dilated cardiomyopathy is a broad term encompassing the phenotypically diverse set of diseases associated with compromised structure and function of the heart (6). DCM is characterized by progressive remodeling of the heart that results in dilation of the left or both ventricles, hypocontractility, and systolic dysfunction with a left ventricular ejection fraction (LVEF) of less than 45% (see **Fig. 1.1**) (4,5,7). While DCM is a complex disease often classified as idiopathic, studies indicate that there are genetic causes in up to 40% of cases (8), and the presence of a genetic cause can contribute to the severity of the pathology. For example, one study found that patients who had advanced DCM that required heart transplantation or a LVAD were more than twice as likely to carry a pathogenic rare variant of a gene associated with DCM (9). Other studies have shown that earlier penetrance, major adverse cardiac events, and end-stage heart failure events occurred in patients positive for pathogenic or likely pathogenic genetic variants (10,11). Moreover, recent work has demonstrated the importance of genetic variants in acquired forms of DCM such as cardiotoxin-induced DCM or myocarditis-induced DCM. Namely, pathogenic genetic variants are present in over 13% of chemotherapy- and alcohol-induced DCM while pediatric myocarditis patients with DCM presentation are genetically enriched for deleterious variants and have lower rates of survival than patients without DCM presentation (12,13). As such, probing the basis of genetically associated DCM cases could help more effectively address some of the most severe presentations of DCM.

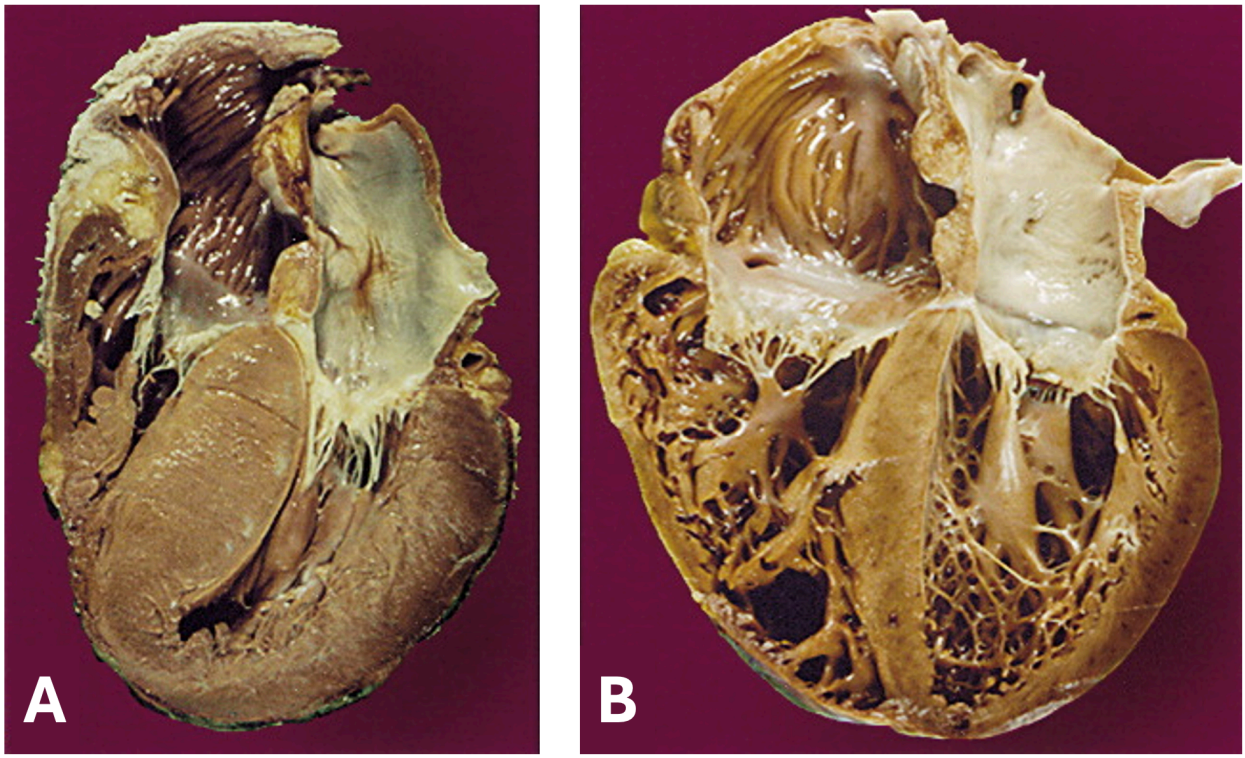

Figure 1.1. A healthy and dilated cardiomyopathy heart.
Compared to a healthy heart (**A**), a heart with dilated cardiomyopathy displays a thinning of the left ventricular wall and a dilation of the ventricular chamber (**B**). *Figure modified from Figure 1 of reference (14).*

Familial cases of DCM, where the patient either has two family members who meet the criteria for DCM or themselves meets the criteria and have a first-degree family member who experienced sudden cardiac death before the age of 35, are frequently reported with an autosomal dominant inheritance pattern (5,15). Mutations in over a dozen genes have been linked to familial DCM (15). Among these, the most common proteins for DCM-associated mutations include lamins A and C, β-myosin heavy chain, and titin (5). These genes are estimated to contribute to 5-8%, 10%, and up to 25% of all familial DCM cases, respectively, and can result in different phenotypes (5,16).

1.1.3 Cardiac myosin variants are particularly potent in dilated cardiomyopathy

While sarcomeric variants make up a significant portion of all pathogenic variants contributing to DCM, they also result in a more severe phenotype than other causes, including faster progression towards heart transplantation and/or death (17). A genetic analysis of pediatric DCM patients performed by Rampersaud et al. revealed that 17 of 19 identified mutations in their population were in sarcomeric proteins, indicating a connection between sarcomeric variants and earlier onset, more aggressive DCM (18). Of the sarcomeric gene variants, β-myosin heavy chain (β-MHC, gene: *MYH7*) mutants can be particularly deleterious, with onset of disease earlier than 18 years of age in roughly 16% of cases, frequent progression to end-stage heart failure, and low rates of left ventricular reverse remodeling in one longitudinal retrospective cohort study (19). Thus, β-MHC mutants pose an interesting and clinically relevant target to study disease-associated variants in order to improve treatment strategies.

1.1.4 Treatments for dilated cardiomyopathy only address symptoms

Historically, physicians treated heart failure and DCM with digoxin and diuretics, both of which managed the fluid retention characteristic of congestive heart failure (20–22). During the late 20th and early 21st centuries, there were several revolutions in heart failure treatments that led to the current standard of care. Moreover, DCM therapeutics are validated in heart failure trials rather than DCM-specific trials since DCM patients tend to have clinical manifestations of heart failure; thus, treatments for dilated cardiomyopathy and heart failure are virtually the same (4). Ultimately, this results in a continued dominance of symptom management rather than slowing or preventing disease progression.

Since the 1980s, several novel classes of therapeutics have demonstrated higher efficacy than digoxin and diuretics at treating heart failure (22). This started with the discovery that treatment

with hydralazine plus isosorbide dinitrate, a combination of drugs that increase vasodilation, reduce mortality in patients with heart failure (22). In the early 1990s, trials demonstrating that angiotensin-converting enzyme (ACE) inhibitors reduce heart failure hospitalizations truly revolutionized heart failure treatment, showing an even higher efficacy than the vasodilators of a few years earlier (22). The late 1990s and early 2000s saw the introduction of angiotensin receptor blockers (ARBs), β-blockers, and mineralocorticoid-receptor antagonists (MRAs) (22). The most recent addition to this set of effective heart failure therapeutics are angiotensin receptor-neprilysin inhibitors, which were demonstrated to be efficacious in 2014 (22). Now, ACE inhibitors and β-blockers are the most common pharmacological treatments for DCM and heart failure (see **Fig. 1.2**), demonstrating the importance of modern pharmacological innovation to better treat DCM (4).

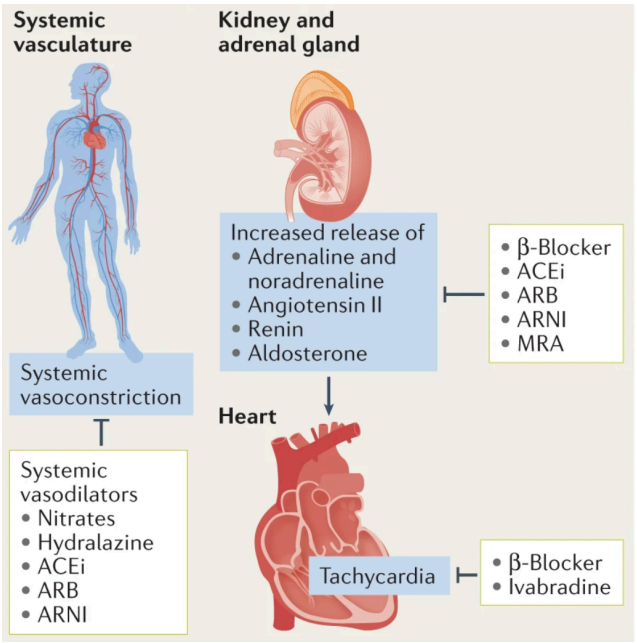

Figure 1.2. Current treatments for DCM and HF address symptoms of disease.
Most treatments for dilated cardiomyopathy focus primarily on the issue of fluid overload by inhibiting the renin-angiotensin-aldosterone system. *Figure adapted from Figure 2 A of reference (23).*

ACE inhibitors impair the conversion of angiotensin I to the active angiotensin II, which is crucial to fibrotic remodeling and pathological fluid retention in DCM (6,22,24). Landmark clinical trials tested the ACE inhibitor enalapril in 253 patients with severe congestive heart failure in the late 1980s and early 1990s (25). Over the course of the 1987 study, the researchers observed a statistically significant 50% decrease in mortality due to the progression of heart failure in the treated group as compared to the placebo group (25). However, it is important to note that this trial was performed in Scandinavian populations that were presumably largely White (race is not even enumerated in the demographic statistics of the sample) and listed as 70% male across both placebo and experimental groups; the lack of diversity in the initial trials does call into question the reliability of results demonstrated by the researchers (25). Several years later in 1991, the same group of researchers studied the effects of enalapril in a much larger sample of over 2400 people with congestive heart failure with LVEF less than 35% (26). In this study, the researchers saw a significant decrease in the number of patients who died or were hospitalized for congestive heart failure in the treatment group as compared to the placebo (26). The replication of the positive effects of enalapril in a larger and more diverse group reinforced the powerful effects of ACE inhibitors, but it is still important to note that roughly 80% of the sample group was White and roughly 80% was biologically male (26). Still, these landmark trials cemented the power of ACE inhibitors as a therapeutic for heart failure, and they are still used as a primary treatment for DCM today. Similar to ACE inhibitors, ARBs inhibit the renin-angiotensin-aldosterone system (RAAS), but they do this through a different mechanism than ACE inhibitors (22). ARBs block angiotensin II's interaction with its receptors but do not block the production of angiotensin II like ACE inhibitors do (22). Since ARBs have had inconsistent efficacy in clinical trials, they are typically only used by DCM patients who cannot take ACE inhibitors (22,27). More recently, trials in 2014

have shown that the angiotensin receptor-neprilysin blocker LCZ696 reduces hospitalization and death as compared to the ACE inhibitor enalapril in a large sample of over 8000 people (27). Neprilysin degrades vasodilating peptides such as natriuretic peptides and bradykinin, so inhibiting neprilysin in addition to angiotensin receptors takes a two-fold approach to limiting systems that result in an increase in cardiovascular pressure and overall stress on the heart in DCM, making it a highly effective treatment for those who cannot take ACE inhibitors (27).

Outside of moderating angiotensin function, β-blockers are another commonly used DCM and heart failure therapeutic. Important studies have shown that the β-blockers bisoprolol, metoprolol, and carvedilol reduce mortality in patients with heart failure, including those with severe heart failure for carvedilol (28–30). However, not all β-blockers have the same mechanisms of action, and some of their effects are complex and not fully elucidated (31). Cells have three different types of β-adrenergic receptors (β_1-AR, β_2-AR, and β_3-AR) (31). Chronic stimulation of β_1-AR as in heart failure can lead to cellular apoptosis, which exacerbates heart damage (31). However, β_3-AR stimulation increases in heart failure and has cardioprotective effects (31). Similarly, if a β_1-blocker is employed, stimulation of β_2-AR increases and could also serve a protective role (31). Bisoprolol and metoprolol are both β_1-selective while carvedilol is β_1- and β_2-selective but slightly prefers to antagonize β_2-AR (28–31). The diversity in β-adrenergic pathways and the affinities of different β-blockers for different receptors leads to a complex set of potential pathways of action, where stimulation of one aspect of the system does not always lead to the same effect. Yet, it is well-established that certain β-blockers modulate these β-adrenergic pathways to improve heart failure outcomes.

The final category of pharmacological treatments commonly used in DCM therapy are MRAs, which directly inhibit the effects of aldosterone by blocking its receptors (32). The use of the MRA

spironolactone in conjunction with an ACE inhibitor and a loop diuretic by the treatment group in one clinical trial resulted in a significant increase in the proportion of the group whose heart failure condition had improved (32). A later trial with the MRA eplerenone demonstrated a significant decrease in heart failure hospitalizations in the treatment group (33). These studies demonstrate that ACE inhibitors do not fully address the RAAS and its role in DCM, and that MRAs hold a rightful place in DCM treatment regimens.

Each of these pharmacological treatments has an important and unique role to play in the treatment of DCM. However, it remains true that these therapeutics address symptoms just as digoxin and diuretics before them—albeit more efficaciously. As DCM progresses irrespective of symptom management, intrusive intervention may be required. For example, an increase in fibrosis can lead to an increase in cardiac arrhythmias, raising the risk of sudden cardiac death (6,34). As such, an implantable cardioverter-defibrillator (ICD), cardiac resynchronization therapy (CRT), or a combination of the two (CRT-D) might be viable treatments. CRT helps resynchronize ventricular contraction when it might be dyssynchronous due to progressive remodeling, which can occur in 15-30% of DCM cases; thus, the therapy improves general quality of life and decreases arrhythmia burden (6,34,35). In contrast, an ICD is designed to prevent sudden cardiac death by preventing bradycardia and resolving dangerous ventricular arrhythmias (34).

Several clinical trials have examined the impacts of ICDs, CRT, and CRT-Ds. An early clinical trial dating back to 2004 measured the impacts of CRT and CRT-Ds. The researchers in this study found that both CRT and CRT-D significantly decreased death or hospitalization from cardiovascular causes as compared to the control group treated with pharmacological therapy (35). The independent effects of both CRT and ICDs were characterized in later trials. In 2005, researchers testing the effects of CRT alone saw a significant decrease in deaths in the CRT and

medical therapy group as compared to the group that only received medical therapy (36). Finally, a clinical trial in 2016 found that people with non-ischemic systolic heart failure (LVEF < 35%) treated with an ICD had a significantly lower occurrence of sudden cardiac death than those in the control group, indicating that the ICD works as designed to reduce the deadly effects of arrhythmias (37). When DCM is such a common cause of arrhythmias, ventricular desynchrony, and sudden cardiac death, CRT, ICDs, and CRT-Ds are vital therapies for many patients.

For patients whose DCM has progressed to an end-stage where their heart's pumping function cannot support their body, only intensive surgical options remain. The two options for those with severe DCM are implantation of a left ventricular assist device (LVAD) or a heart transplantation (4,34). Clinical trials have found that use of a LVAD for at least a year significantly increased survival in people with end-stage heart failure as compared to those who only received medical therapy (38). For many, LVAD serves as a bridge to transplantation, which can be incredibly difficult to access (34). The sad truth remains that though pharmacological therapies can slow down the progression of disease to some extent and implantable devices can reduce the risk of sudden cardiac death, DCM still often progresses to this tragic end stage with very limited options for care. Thus, a better understanding of the pathogenesis of DCM is crucial to informing a novel class of therapeutics with the ability to inhibit DCM progression altogether and improve outcomes.

1.2 Current methods to study dilated cardiomyopathy pathogenesis

1.2.1 Animal models

Animal models have been used for several decades to study DCM and continue to be used today. Small animal models, particularly rodents, are often used in preliminary studies since they are less expensive and easier to manage in larger samples than large animal models (39). In contrast, large

animal models such as pigs are used after basic sciences discoveries are ready to enter the translational stage of medical research (39).

Certain small animal models, such as the BIO14.6 and CHF 147 strains of hamsters, naturally develop dilated cardiomyopathy and can be used to study the pathogenesis of the disease (39). Alternatively, researchers can genetically modify mice to study the effects of specific mutations on the progression of DCM (39,40). There are high numbers of mouse models because 99% of human genes have an ortholog in mice, making it relatively easy to generate transgenic and knockout lines expressing mutations associated with DCM (39,40). To date, there have been mouse models with mutations in lamin, troponin, titin that have demonstrated a DCM phenotype (40,41). However, the efficacy of mouse models does not extend to the study of β-myosin variants because mice primarily express the faster α-myosin heavy chain ATPase in their hearts while humans primarily express the slower β isoform (40). Moreover, a mouse's heart is much smaller than a human heart, so this model system cannot be entirely accurate.

Despite these limitations, the power of animal models is that they allow for the study of disease *in vivo*. For example, echocardiography and magnetic resonance imaging can be performed on rat models, mirroring the same diagnostic tests used on humans to assess DCM (40). Several other sets of data can be extracted from animal tissue. For example, isometric force and the rate of tension redevelopment can be derived from permeabilized tissue mechanics, and additional structural data can be surmised from X-ray diffraction experiments (42). These data provide valuable insight into the cardiac system, making animal models a vital part of cardiac bioengineering approaches.

1.2.2 Stem cell models

As previously discussed, though animal models provide the only avenue for *in vivo* studies of DCM, the physiology of small animal models does not recapitulate human physiology, and large animal models are too expensive to use with high frequency (40). Additionally, human myectomy samples can be hard to obtain and frequently show late stages of a disease since they are extracted during other surgeries that are often performed on people with end-stage heart failure (43). Stem cells are unique in that they have differentiation potential into various cell types and are self-renewing, which could solve current issues with animal models and human samples by providing a reliable source of human cells that can be studied. However, early studies were only possible with embryonic stem cells, which pose ethical dilemmas.

In the early 2000s, Dr. Shinya Yamanaka revolutionized stem cell research by reporting the production of induced pluripotent stem cells (iPSCs) from somatic cells (44). By making somatic cells express 4 transcription factors (*OCT4*, *SOX2*, *KLF4*, and *c-MYC*) associated with pluripotency, Dr. Yamanaka developed a way to achieve the benefits of a stem cell system—namely, the use of human cells and the self-renewal capabilities—without the ethical quandary related to embryonic stem cells (44,45).

The first models of DCM in iPSCs were in patient-derived iPSCs. In 2012, Sun et al. demonstrated the successful reprogramming of skin fibroblasts from a family with the DCM-associated cardiac troponin T mutation R173W into iPSCs that they subsequently differentiated into a cardiovascular lineage and subsequently into spontaneously beating embryoid bodies (46). Patient-derived iPSCs have also been generated for the desmin mutation A285V and the lamin A/C mutation R225X and have been differentiated into cardiomyocytes in spontaneously beating embryoid bodies via coculture with endoderm-like cells (47,48). Each of these studies demonstrated a variety of

experimental procedures to analyze the mutant iPSC-derived cardiomyocytes (iPSC-CMs), including imaging for sarcomere structure, patch clamp studies to assess electrophysiology, and calcium handling (46–48). Work with patient-derived iPSCs highlights the power of stem cell models to demonstrate a significant difference in the characteristics of wild type cells and pathogenic mutant cells. Analytical methods probing various aspects of iPSC-CM contractility and structure provide a multifaceted and nuanced view of how a specific mutation might be impacting the cell, allowing researchers to better understand the pathophysiology of DCM on a cellular scale.

In recent years, the rise of clustered regularly interspersed short palindromic repeats (CRISPR)/Cas9 gene editing technology has proven very valuable for cardiac disease modeling. This approach to gene editing has gained traction due to its high specificity, efficiency, and customizability as compared to other approaches (49). In many ways, the CRISPR/Cas9 system is also easier to use than other gene editing methods like transcription activator-like effector nucleases (TALENs), which requires more effort on the part of the researcher to target to new editing sites (49). As an overview, the CRISPR/Cas9 system leverages a guide RNA that targets the complex to the desired editing site in the DNA, where the Cas9 nuclease will create a double-stranded break that can be fixed by homology-direct repair, which is based off of a template for a desired change, or non-homologous end joining, a more error-prone strategy (49). Modifications in the CRISPR system have also allowed for the advent of base editing, which can make a single-nucleotide substitution without introducing a double-stranded break, and prime editing, where a prime editing guide RNA (pegRNA) can be used as a template for a substitution or insertion without a double-stranded break (49). In disease modeling, the CRISPR/Cas9 system can be used to introduce a pathogenic mutation into a control iPSC line or to correct a pathogenic mutation in patient-derived iPSCs (49,50). These methods can be used to engineer new, severe mutations that

might not be found in nature to better understand the molecular mechanisms of DCM or to develop a gold standard for an isogenic control for studies of a mutant DCM-associated cell line (51). As such, the CRISPR/Cas9 gene editing technology is already making a difference in DCM studies and will continue to do so as the technology improves and is further engineered to maximize efficacy and minimize off-target effects (50).

Despite the various successes of *in vitro* iPSC-CM models for dilated cardiomyopathy, it is important to note that this model system, like animal model systems, has limitations. Primarily, the largest deficit of iPSC-CM model systems is their lack of maturity, demonstrating a fetal cardiomyocyte phenotype rather than an adult phenotype (52). For example, iPSC-CMs tend to be smaller in size with lower membrane capacitance, higher resting membrane potential, irregular morphology, and sarcomeric disarray as compared to adult cardiomyocytes (52). These characteristics lead to inefficient excitation-contraction coupling, resulting in lower force production (52). They also tend to be metabolically immature, relying on glycolysis rather than the fatty acid β-oxidation strategy that adult cardiomyocytes use (52). Currently, there are many ongoing efforts to improve iPSC-CM maturity so that they can serve as a better model system for DCM and other cardiomyopathies. These strategies include supplementing iPSC media with fatty acids and growth factors design to improve metabolic maturity and coculture with other cell types like fibroblasts and endothelial cells (53). Additionally, growing the cells on micropatterned or grooved substrates can improve sarcomere structure (52). However, it is important to note that despite these advances, iPSC-CMs treated with these methods are still relatively immature (52).

Currently, the field addresses the gaps in immaturity in 2D cultured iPSC-CMs through the development of engineered heart tissues (EHTs). EHTs are constructed based on the principle of mimicking the 3D environment the heart to more accurately recapitulate maturity and function of

the cardiomyocytes cultured in the EHT (51). EHTs are commonly made of a mixture of cardiomyocytes, fibroblasts, and endothelial cells in a hydrogel scaffold (54,55). Several different types of EHTs can be constructed, including cardiac strips, which are suspended between PDMS pillars to measure contraction parameters (56). These can be further matured through mechanical stretching and electrical stimulation to achieve the current gold standard in iPSC cardiac modeling (53). This enhanced maturity and more representative structure often translates into better experimental results. As compared to single cell measurements, which often have high variability in the results that limits reproducibility, EHTs have previously demonstrated superior ability to detect differences between wild type and pathogenic variants (57). For example, researchers studying DCM-causing titin mutations saw that while they were not able to see a difference in contractile properties when studying single cells, they were able to see a significantly lower twitch force in an EHT made with mutant iPSCs as compared to wild type iPSCs (57). Though they are more expensive and time-intensive to create, it is necessary to leverage EHTs to study DCM because much of the disease is related to extracellular cues from extensive fibrosis. By modulating the properties of the scaffold and the genetic makeup of cardiomyocytes used in the EHT, researchers will be able to better understand how the environment exacerbates cell dysfunction and how cell dysfunction relates to adverse extracellular matrix remodeling.

1.2.3 Computational models

When calcium is released from the sarcoplasmic reticulum as a result of an action potential depolarizing a cardiomyocyte, it can bind to a protein called troponin C that is complexed to troponin I, troponin T, tropomyosin, and actin in the thin filament (58). This causes tropomyosin to shift positions, exposing myosin-binding sites on actin (58). Myosin can then interact with actin in the crossbridge cycle, hydrolyzing ATP and releasing the hydrolysis products to generate force

(58). Given the complex protein-protein interactions involved in contraction, it stands to reason that mutations in any of these proteins could influence the dynamics of muscle contraction, resulting in a disease phenotype of contractility. Studying the motions of single proteins experimentally is challenging due to the minute scale, but computational models can bridge this gap and help researchers better understand the normal function of the sarcomere as well as the impacts of pathogenic mutations.

One form of computational protein analysis frequently used to study the sarcomere and its component proteins is molecular dynamics (MD). MD simulations have been part of research since the mid-20th century, but they have exploded in recent years due to increases in the number of resolved protein structures and improvements in computer hardware and MD software (59). MD simulations use Newton's laws of motion to calculate how the position of each atom in a protein structure changes over a series of timesteps, generating a trajectory that provides spatiotemporal data at a time resolution of femtoseconds to picoseconds (59). Like many other computational methods, MD's strength is that the system can be perturbed relatively easily and the effects of that perturbation can be analyzed on an atomic scale (59). In this way, a wild type MD model of a sarcomeric protein could have a DCM-causing mutation introduced into it, and the dynamics of the modified protein could be assessed to predict the changes that mutation might cause in the contractility of a patient's heart.

The field of cardiac bioengineering has embraced MD, and several research groups across the world have used it to assess the standard molecular mechanisms of cardiac contraction as well as the impacts of several DCM-associated mutations. For example, Kawakubo et al. used MD to simulate hydrolysis of ATP to ADP and phosphate in the nucleotide binding pocket of myosin and were able to identify several key residues impacted by ATP hydrolysis and to observe that the

myosin head had biased swinging motions around the hinge with the level arm when it was fixed as it would be in the thick filament (60). Such analysis could be used to study different steps of the crossbridge cycle to note patterns in wild type protein behavior. Only by first understanding the wild type can researchers draw conclusions about mutant protein structures.

In studying mutant protein structures, many groups have focused on tropomyosin, which is essential for regulating the actomyosin interaction that forms the basis of contraction (58). In particular, MD has been used to study two well-established mutations in tropomyosin that are associated with DCM, M8R, and K15N (61). One study demonstrated that these mutations decreased the number of hydrogen bonds in the overlap junction between two tropomyosin molecules, destabilizing the tropomyosin-actin complex; they concluded that a decrease in the stability of this tropomyosin-actin complex, impairing regulation of muscle contraction and providing a molecular mechanism for the hypocontractile phenotype caused by these mutations (61). Another group using MD to study the M8R mutation in a model of an infinite cable of tropomyosin saw that the mutation decreased the stiffness of the tropomyosin overlap junctions and distorted the structure into a conformation that would block myosin binding to actin better than the wild type (62). These studies provide a framework for the use of molecular dynamics in assessing the effects of mutations on protein structure, demonstrating that computational models have deep relevance to the pathogenesis of complex cardiac diseases.

As previously mentioned, the origin of roughly 40% of DCM cases is genetic, but it can be challenging to identify disease-causing mutations if they are previously undocumented or to understand the pathophysiology associated with a specific mutation once it is identified (6). The flexibility of a computational model like MD to perturb a system with any number of mutations allows researchers to identify potential impacts of variants of unknown significance, determine

their pathogenicity, and hypothesize their effects on contractility (63). Additionally, MD can help predict the mechanisms of previously identified pathogenic mutations in order to guide experimental studies *in vitro* and *in vivo*. Taken all together, computational models are a valuable tool to study the causes of genetically associated DCM and can help streamline studies of specific mutations, making them indispensable to accelerating the growth of institutional knowledge about this disease.

1.3 Relevant mechanisms of cardiac muscle regulation

When an action potential propagates through cardiomyocytes, membrane depolarization results in the opening of voltage-gated calcium channels (58). As calcium enters the cell, it can bind to ryanodine receptors, triggering release of calcium from the sarcoplasmic reticulum in a phenomenon known as calcium-induced calcium release (shown in **Fig. 1.3**) (58). When intracellular calcium is high, it binds to a regulatory protein called troponin C in the thin filaments; this causes troponin C to change configuration and shift another regulatory protein called tropomyosin to expose myosin-binding sites on actin (58). Once myosin binds to actin, it can initiate the powerstroke, in which phosphate and ADP are released from the nucleotide-binding pocket to generate force in what is known as the sliding filament theory of contraction (**Fig. 1.4**) (58). This is the general mechanism of cardiac muscle contraction, but this system consists of several key regulatory and contractile proteins implicated in healthy myocardium function. These proteins and their role in contractile regulation are enumerated below.

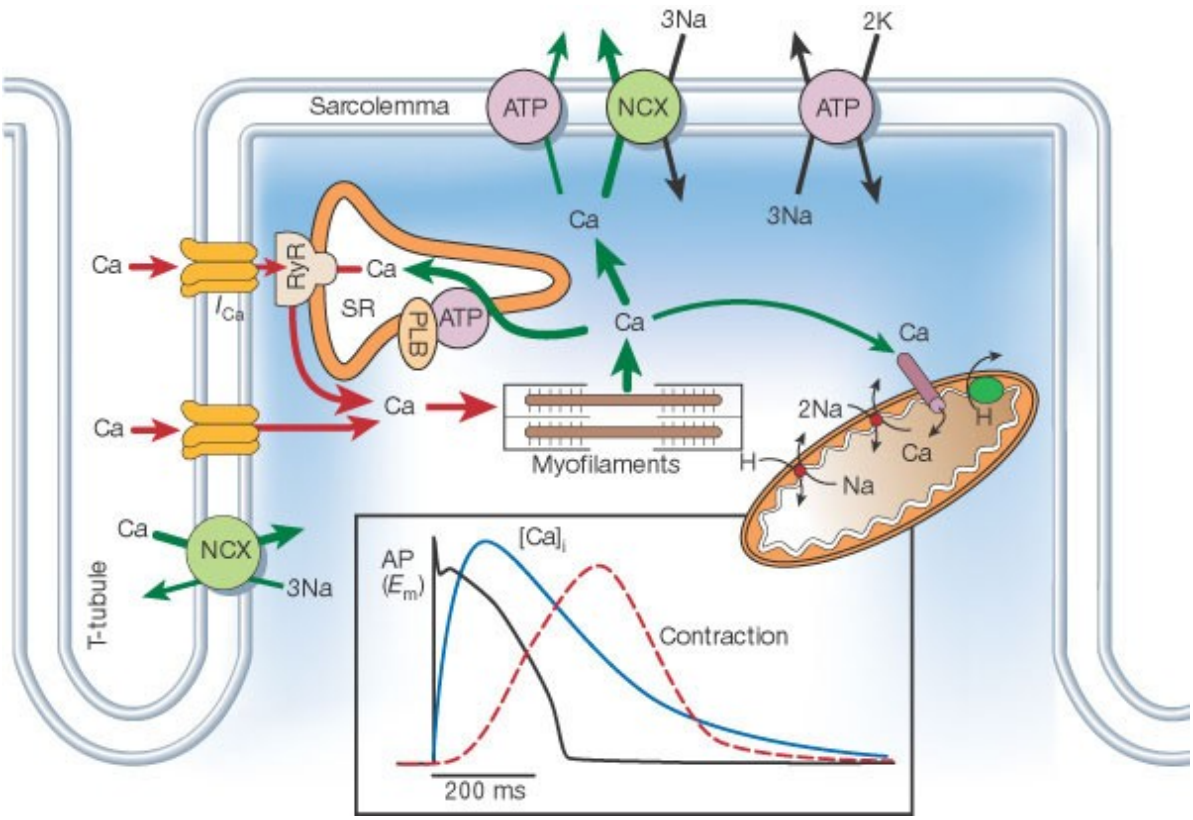

Figure 1.3. Calcium-induced calcium release in cardiomyocytes.

When an action potential results in a depolarization of the cell membrane, voltage gated calcium channels open and allow calcium into the cell. This calcium can bind to ryanodine receptors (RyR) on the sarcoplasmic reticulum (SR) to release calcium into the cytosol, where it can bind to troponin complexes in the sarcomeres to facilitate contraction. Relaxation is facilitated by a return to basal calcium levels, which is modulated by the SR Ca^{2+} ATPase, sarcolemmal sodium-calcium exchangers (NCX), sarcolemmal Ca^{2+} ATPases, and mitochondrial uptake. *Figure adapted from Figure 1 of reference (64).*

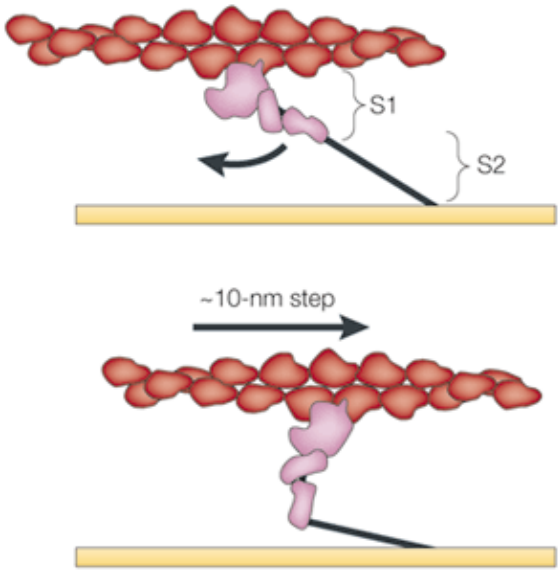

Figure 1.4. The sliding filament theory of contraction.
In the sliding filament theory of contraction, S1 heads bind to actin filaments, and the subsequent release of phosphate and ADP from the nucleotide-binding pocket of myosin leads to the swinging of the lever arm and generation of force. *Figure adapted from Figure 1 of reference (65).*

1.3.1 Myosin and thick filament regulation

The motor protein β-myosin heavy chain is a key component of the contractile machinery of the sarcomere (16). Myosin decorates the thick filaments of the sarcomere and is made up of a long tail and two S1 heads which each contain an actin-binding surface and a nucleotide-binding pocket as well of several functional domains (**Fig. 1.5**) (58,66). The molecular events underpinning the sliding filament theory are described by the crossbridge cycle (**Fig. 1.6**). In this cycle, myosin has a variety of roles, including binding to actin, facilitating release of ligands from the nucleotide-binding pocket, and swinging the lever arm. Given this level of complexity, it is understandable that disease-associated mutations can occur anywhere in the myosin protein. For example, one study of DCM patients found molecular variants in myosin at residues 120, 412, and 550, among

others (67). These residues are located in the N-terminal domain of myosin, the actin-binding surface in the upper 50 kDa domain, and the actin-binding surface in the lower 50 kDa domain, respectively, but they lead to a similar hypocontractile phenotype. This heterogeneity illustrates the necessity of studying disease pathogenesis on a mutation-by-mutation basis. Furthermore, a close examination of such mutations often reveals heterogeneity in the specific steps of the crossbridge cycle affected by a mutation. For instance, Ujfalusi et al. demonstrated that five different DCM-causing mutations had differential effects on short S1 (sS1) affinity for actin as well as binding affinity of sS1•actin complex for ATP and ADP (68). Thus, a variety of combinations of a mutation's effects on the different kinetic parameters of the crossbridge cycle can lead to the same disease.

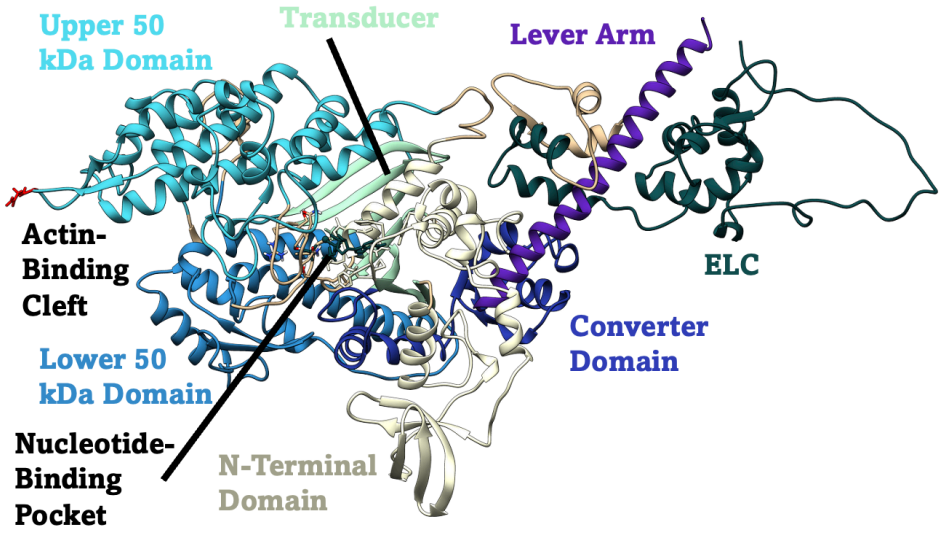

Figure 1.5. The functional domains of the cardiac myosin motor domain.
Cardiac myosin's actin-binding surface is made up of the upper and lower 50 kDa domains. The lower 50 kDa domain is responsible for initial electrostatic interactions, and cleft closure via the upper 50 kDa domain facilitates strong binding. Movement of the transducer region causes shifts in the N-terminal and upper 50 kDa domains, resulting in release of ADP. All of these structural changes are transmitted to the lever arm via the highly flexible converter domain, allowing for the swinging of the lever arm and force generation (66). This structure also includes the essential light chain (ELC), a regulatory component.

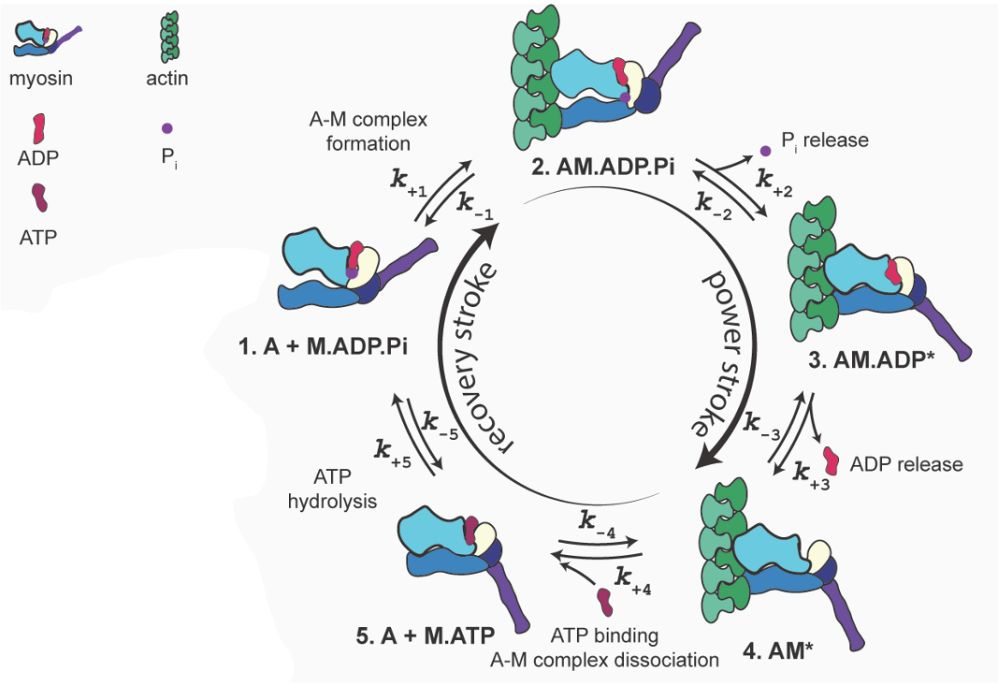

Figure 1.6. The crossbridge cycle of muscle contraction.

In the crossbridge cycle, myosin heads first form a weak interaction with actin. Next, movement in the transducer region result in phosphate release and transition to the strongly bound state. This comes along with swinging of the lever arm in the powerstroke to generate force. ADP release leaves the actomyosin complex intact in a non-force-producing state. Finally, binding of ATP allows the lever arm to return to its original conformation, and hydrolysis of that ATP re-primes the lever arm in the recovery stroke. *Illustration by Dr. Matthew Childers, Regnier Lab, University of Washington (2023).*

While it is crucial to examine the crossbridge cycle when studying disease pathogenesis, thick filament regulation also plays a role in force-generating capability. Myosin motors are generally thought to occupy two distinct biochemical states with different capacities to bind actin and generate force: the disordered relaxed state (DRX) and the super relaxed state (SRX). In SRX, the blocked and free heads of a myosin dimer are bound together in the interacting heads motif (IHM) structural state via intramolecular interactions and additionally folded back against the core of the thick filament, making them less accessible for binding to actin (see **Fig. 1.7**) (69). The

inaccessibility of actin to the free heads in SRX is what leads to the characteristic decrease in ATPase activity as compared to DRX (69,70). Myosin DRX—where the free head is liberated—is accessible upon destabilization of the IHM, which can occur via phosphorylation of the regulatory light chain or cardiac myosin-binding protein C (69). In the context of DCM pathogenesis, recent work by Rasicci et al. has demonstrated that the DCM-associated myosin mutation E525K dramatically stabilizes the IHM, leading to a DCM phenotype despite the fact that ATPase catalytic activity is increased (71). In this way, mutations that impact head-head intramolecular interactions or head-S2 intra- or intermolecular interactions can alter the ratio of SRX to DRX myosin heads, modulating force generating capacity and leading to a disease phenotype.

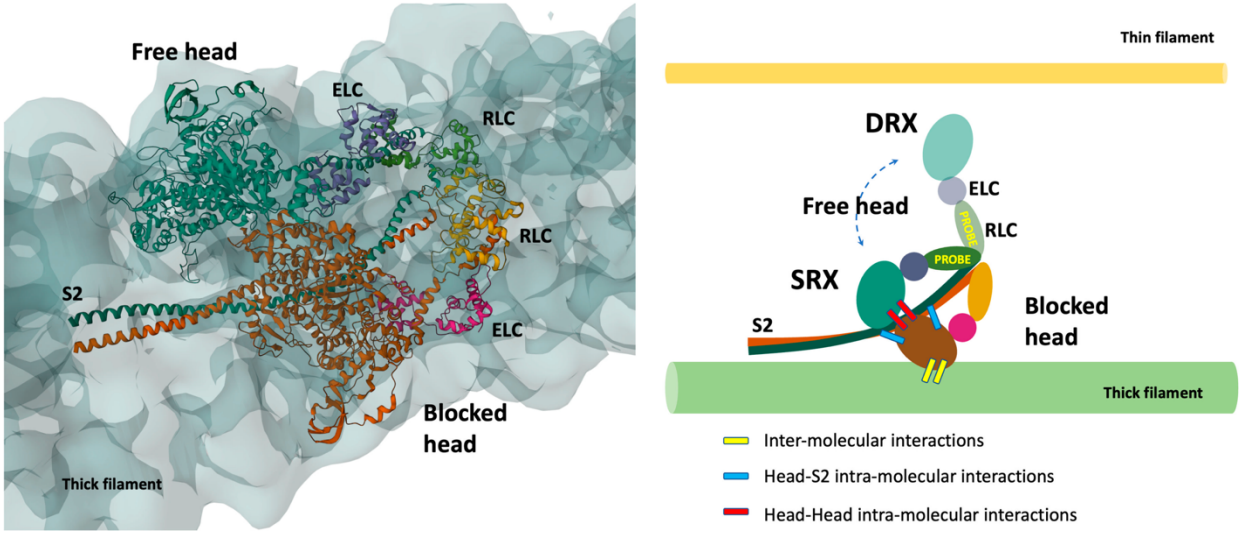

Figure 1.7. The relationship between IHM, SRX, and DRX in thick filament regulation.
The interacting heads motif (IHM, left) is a structural state in which the blocked and free heads of a myosin dimer are bound via intramolecular interactions. The IHM is associated with the biochemical super relaxed state (SRX), which is defined by decreased ATPase activity via a sequestering of blocked and free heads along the thick filament backbone. When the IHM is destabilized and head-head interactions are disrupted, the free head is available to bind to actin, resulting in transition to the disordered relaxed state (DRX) and greater force generation capacity. *Figure adapted from Figure 2 of reference (70).*

1.3.2 Troponin and tropomyosin in thin filament regulation

While actin is the protein to which myosin heads bind to generate force, myosin access to actin is governed by tropomyosin and the troponin complex. Tropomyosin is an α-helical coiled coil consisting of seven pseudo-repeats that spans seven monomers of actin (72). For each heptad of actin, there is one tropomyosin molecule and one troponin complex. Calcium can bind to the troponin complex, resulting in a shift of tropomyosin away from myosin-binding sites on actin, freeing them for actomyosin complexing (72).

The troponin complex is calcium sensitive and thus the primary point of contraction regulation in the thin filament. The cardiac troponin complex is made up of three subunits denoted as troponin C (cTnC), troponin I (cTnI), and troponin T (cTnT). cTnC is the subunit to which calcium binds to initiate contraction. In cardiac muscle, the primary calcium binding site for contractile regulation is known as site II (72,73). When calcium binds to site II, helices in cTnC reorient and expose hydrophobic residues, leading to stronger contact formation between cTnC and cTnI (72,73). While cTnI's primary function is to inhibit contraction, the movement of the inhibitory peptide of cTnI in response to calcium binding to cTnC allows for the translocation of tropomyosin and increased accessibility to myosin-binding sites (see **Fig. 1.8**) (73–76). The third subunit, troponin T, is thought to hold together the interactions between the various thin filament proteins and to communicate structural changes from calcium binding to cTnC to the rest of the thin filament to facilitate efficient regulation (72,77).

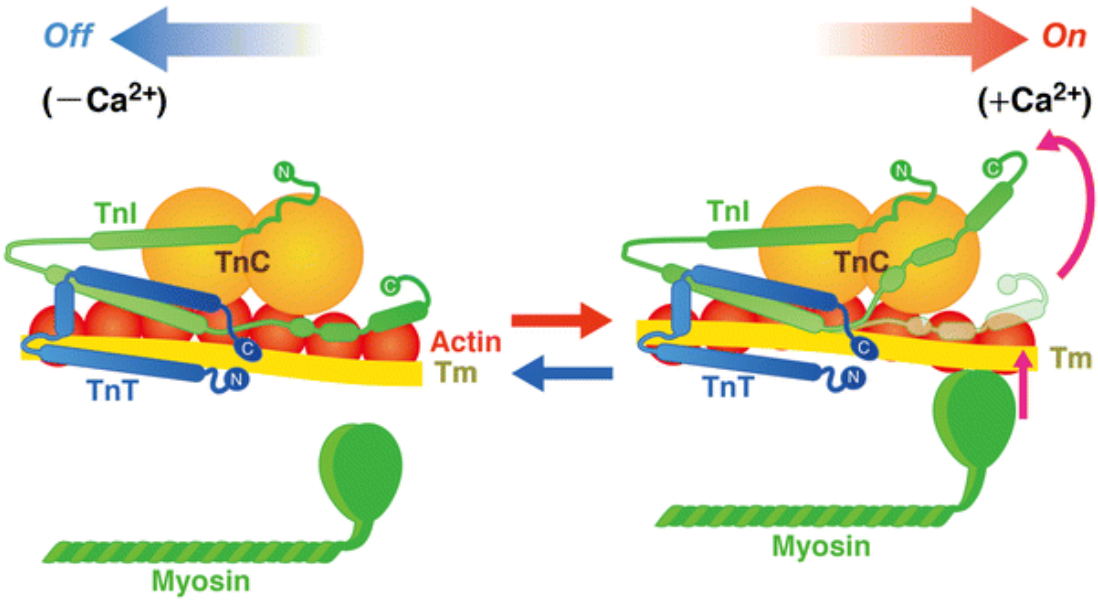

Figure 1.8. Troponin regulation of actomyosin binding.

When calcium binds to cTnC, the C-terminus of cTnI can dissociate from its binding site on actin to associate more closely with cTnC. As a result, tropomyosin can shift along actin, opening binding sites for actomyosin binding. *Figure adapted from Figure 3 of reference (74).*

As tropomyosin moves in response to changes in troponin conformation, its position can be described by the three-state model. In this paradigm, tropomyosin occupies the "blocked" ("B") state in the absence of calcium and prevents myosin binding to actin (78–80). When intracellular calcium increases, the aforementioned change in troponin conformation allows for tropomyosin to shift azimuthally 25º relative to actin, occupying the "closed" ("C") position in which weak actomyosin interactions are possible (78–80). A small proportion of these weakly bound crossbridges can transition to a strongly bound complex, and this transition is thought to mediate the transition of tropomyosin to the "open" (also known as "myosin," or "M") state through a further 10º azimuthal shift along the actin filament (79,80). Myosin's involvement in this final transition illustrates a clear pathway through which a mutation in myosin can alter thin filament regulation.

This is doubly true because there is a secondary level of thin filament regulation governed by a cooperative mechanism in which crossbridge formation and translocation of tropomyosin to the M state facilitates the activation of neighboring tropomyosin molecules and the capacity for crossbridge formation on the newly exposed myosin-binding sites of actin (79). Thus, if a mutation in myosin alters the motor domain's capacity to interact with the thin filament, the attenuation of this cooperative mechanism would lead to decreased crossbridge formation and decreased force production.

While thick and thin filament regulation of contraction are described as separate here, it is important to note that these processes are inherently coupled by the fact that they both implicate myosin. Any change to the free S1 head's interaction with the blocked head may result in allosteric changes that alter thin filament cooperativity and vice versa. As such, it is necessary to consider the whole contractile apparatus when considering disease pathogenesis.

1.4 Our system of interest: the likely pathogenic β-MHC mutation R369Q

The R369Q mutation is a missense mutation where a single nucleotide base pair change in DNA from guanine to adenine results in an amino acid change from the positively charged arginine to the polar, but uncharged, glutamine. It is located on loop 4 of the actin-binding surface of cardiac myosin (**Fig. 1.9**).

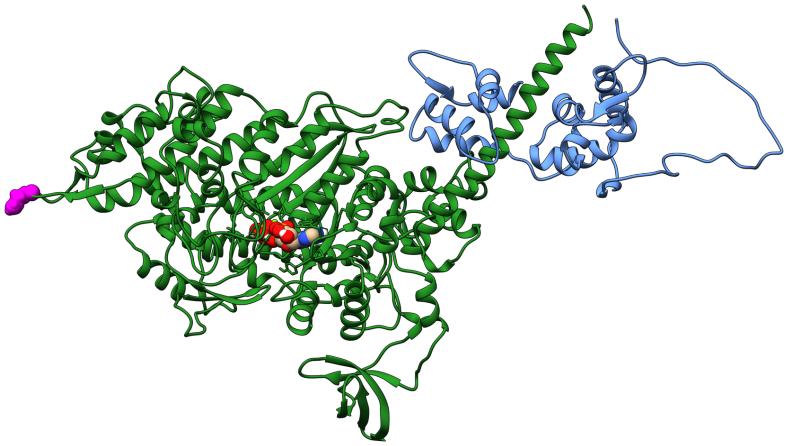

Figure 1.9. The R369Q mutation is located on loop 4 of the cardiac myosin structure.
The R369 residue (magenta) is located on loop 4 of the myosin structure. An alteration in charge on the actin-binding surface could modulate electrostatic interactions with the negatively charged actin filament.

1.4.1 Cases of R369Q in DCM patients

The R369Q mutation is classified as likely pathogenic for primary dilated cardiomyopathy by a cardiomyopathy variant curation expert panel. According to panel criteria for *MYH7*-associated cardiomyopathies, the R369Q mutation meets one strong indicator for pathogenicity (identification in ≥15 probands) as well as two moderate indicators (absence from large-scale studies, existence as a *de novo* mutation) and one supporting indicator (variant segregates in ≥3 people with disease) (81–87). This level of criterion satisfaction corresponds to a high likelihood that this mutation is associated with disease and means that identification of the mutant in genetic testing can inform clinical decisions. Notably, one index patient with the R369Q mutation was only five at the age of diagnosis and required a heart transplantation at age 22, supporting the fact that *MYH7*-related cardiomyopathies are particularly potent (82).

1.4.2 Prior work on loop 4 and R369Q

While the R369Q mutation has been established as a likely pathogenic variant of β-MHC, there have been limited studies on the mechanism by which this mutation leads to the typical hypocontractile phenotype.

Work by Dr. Bill Lehman's lab at Boston University has illuminated the structure of β-MHC using cryo-electron microscopy (cryo-EM) and computational techniques (88,89). Particularly, the resolved cryo-EM structure for recombinant myosin bound in rigor to an actin-tropomyosin complex shows a close interaction between loop 4 and adjacent tropomyosin residues, with molecular modeling further predicting a highly promiscuous loop 4 that facilitates tropomyosin transition to the M state and impedes return to the C state (88–90). Therefore, structural studies demonstrate a role for loop 4 and R369 in activating the thin filament and slowing deactivation.

Currently, there exist no functional studies on the R369Q mutation in animal or cell models. Trujillo et al. studied the role of the R369 residue in muscle regulation in *Drosophila melanogaster* by mutating the amino acid to a histidine, a similarly charged residue that is much more rigid than arginine (91). While this study was not performed with our mutation of interest, it still provides insight into the role of the R369 residue and how perturbing it could lead to muscle dysfunction. Specifically, the authors saw that this mutation decreased maximal S1 binding to actin but otherwise had no effects on cardiac muscle structure or organ-scale function (91). Though the R369Q mutation is acknowledged to be likely pathogenic, experiments to connect structure and function in the mutation's effects are still absent from the field, and studies that examine the residue are in the *Drosophila Mhc* myosin gene, which only holds about 55% sequence similarity with the human β-MHC gene *MYH7* (92). These gaps in knowledge surrounding the R369Q

mutation further illustrate the pressing need to understand its effects in a context more physiologically relevant to the human heart.

1.4.3 A hypothesis for R369Q's role in DCM pathogenesis

While there have been no *in vitro* studies of R369Q in human cells, recent computational work performed by our group in collaboration with Dr. Bill Lehman's lab at Boston University suggests a role for the R369 residue in thin filament activation. Extending the aforementioned structural work on loop 4 performed by Doran et al., our groups' collaborative effort generated steered molecular dynamics simulations depicting the transition from pre-powerstroke to post-powerstroke myosin in a myosin-tropomyosin-actin complex (93). These simulations showed that loop 4 was responsible for shifting tropomyosin towards the M state via charge-charge repulsion between loop 4 charged residues R369 and K367 and tropomyosin charged residues R101, R105, and K112 (see **Fig. 1.10**) (93).

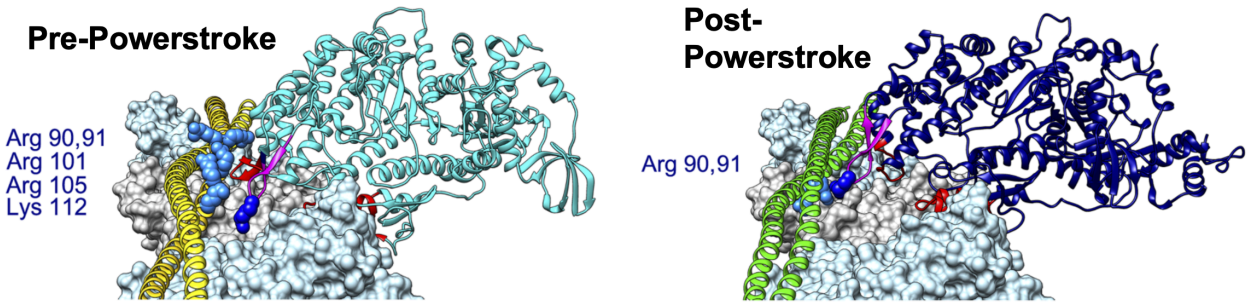

Figure 1.10. Myosin-tropomyosin charge-charge repulsion.
In the pre-powerstroke state, R369 (dark blue spheres), located on loop 4 (magenta) of myosin (cyan), repels positively charged residues (light blue spheres) on tropomyosin (yellow). In the post-powerstroke conformation, tropomyosin has shifted azimuthally and R369 (dark blue spheres on navy blue myosin) repels a different set of positively charged residues (light blue spheres) on tropomyosin (now depicted in green). *Figure modified from Figure 2 C-D of reference (93).*

To confirm loop 4's involvement in thin filament activation, the authors also generated steered MD simulations for with an S1 mutant that replaced the seven polar and charged residues on the tip of loop 4 with glycine, the smallest nonpolar amino acid (93). These simulations reflected a reduced displacement of tropomyosin from the C to the M state, suggesting a higher barrier to motor head cleft closure (93). Decreasing probability of the pre- to post-powerstroke transition by reducing charge-charge repulsion impedes strong crossbridge attachment and associated thin filament cooperativity mechanisms, suggesting the primary effect of the R369Q mutation is altering myosin-thin filament interactions to reduce activation of the thin filament and force generation. The present work seeks to dissect if this proposed mechanism is further supported by *in vitro* work as well as further molecular dynamics simulations.

1.5 Project overview

The heart is a complex multiscale organ whose contractile function is governed by layers of electrical, mechanical, and biochemical regulation. As such, the heart can—and must—be studied from a multiscale perspective in order to understand the whole scope of a mutation's effects on cardiac function. To this end, this project aims to develop an understanding of the phenotypic effects of the R369Q mutation in a translationally applicable stem cell-derived cardiomyocyte model and leverage reductionist assays and computational simulations to explain these results from a mechanistic standpoint. In pursuit of this goal, the project can be broken up into **two aims:**

> **Aim 1:** To use a human induced stem cell derived-cardiomyocyte model to examine the phenotypic effects of the R369Q mutation in cell- and tissue-scale systems with the intact endogenous cellular contractile machinery.

Aim 2: To pinpoint specific aspects of the crossbridge cycle, thick filament regulation, and/or thin filament regulation affected by the R369Q mutation by interrogating patterns in myofibril kinetics and altered protein dynamics in molecular dynamics simulations.

The completion of this project serves as an example of the power of multiscale approaches and the diversity of regulatory information provided at each level. Such a pipeline could be applied to other sarcomeric mutations associated with inherited cardiomyopathies and inform a vast array of highly targeted therapeutics as society moves into an era of personalized medicine that addresses the source of pathologies rather than the symptoms.

Chapter 2

Elucidating the R369Q Mutation's Phenotypic Effects in Cell- and Tissue-Scale Systems

2.1 Introduction

The 21st century has seen the revolutionization of disease modeling with the advent of induced pluripotent stem cells and CRISPR/Cas9 technologies to methodically introduce mutations into the genetic code of these cells. Human induced pluripotent stem cell-derived cardiomyocytes (hiPSC-CMs) are a valuable model system for studying cardiac pathologies because they can express the proper β isoform of myosin without the intensive and expensive process of developing an efficient transgenic animal model—particularly larger models such as pigs, which better represent the human heart but can prove challenging to generate (40). While myectomy samples offer the benefit of mature cardiac tissue, they are not readily available since they are only extracted in the context of heart surgery—an intervention only carried out after drastic progression of disease (43). The rarity of such samples as well as the effects of years of cardiac remodeling and potential genetically associated comorbidities precludes the efficacy of myectomy samples as an efficient, reliable source of human cells as a disease model. As such, hiPSC-CMs provide an attractive alternative to study diseases in a dish.

While hiPSC-CMs' inherent immaturity poses a challenge to their translational capacity as a model system, recent years have seen the development of methods to improve cardiomyocyte maturity and thus the model system. Chief among these is the development of engineered heart tissues

(EHTs), which leverage 3D culture methods wherein hiPSC-CMs are embedded in an extracellular matrix protein-derived hydrogel incorporating supporting architecture from other cells to improve maturation and better represent the effect of systemic perturbations such as introduced mutations (51,53,57). Such EHT models have demonstrated efficacy at discerning contractile differences between wild type EHTs and those with cardiomyocytes harboring a pathogenic mutation (57). The improved maturity of these EHT constructs prompts consideration of this model system to study the effects of pathogenic mutation.

On a more granular scale, prior work has demonstrated that culturing hiPSC-CMs on micropatterned polyacrylamide gels improves their mechanical output and strengthens the relationship between sarcomere shortening and force generation (94). By leveraging an iPSC line that labels the Z disks of sarcomeres, Ribeiro et al. were also able to demonstrate accurate detection of changes in sarcomere shortening as a result of under the conditions of different inotropic drugs (95). This cell culture and experimental paradigm therefore serves as a valuable tool to better understand how perturbations in a cellular system—such as the R369Q myosin mutation—can translate to altered force generation.

This aim seeks to leverage cutting-edge techniques for cardiomyocyte maturation and combine analysis from engineered heart tissues and micropatterned hiPSC-CMs in order to better understand the phenotypic effect of the R369Q mutation.

2.2 Methods

2.2.1 Differentiation of induced pluripotent stem cells into cardiomyocytes and subsequent maturation

CRISPR/Cas9-edited stem cells with a homozygous *MYH7*$^{R369Q/R369Q}$ mutation were obtained from the Allen Institute for Cell Sciences in Seattle, Washington. Importantly, these cells incorporated an α-actinin GFP tag that allowed for fluorescent imaging of the Z disks of sarcomeres (96).

We differentiated and purified these cells according to previously established protocols modulating the WNT signaling pathway with modifications to improve differentiation efficiency (**Fig. 2.1**) (97,98). Briefly, stem cell lines were seeded into 12-well plates coated with Matrigel® (356231, Corning) at densities ranging from 30,000 to 70,000 cells per well on what is considered Day -2 of the protocol. On Day -1, the cells were fed mTeSR1 media (85850, Stemcell Technologies) supplemented with 1 μM CHIR99021 (13122, Cayman Chemical). On Day 0, the basal media was changed to RBA basal medium consisting of RPMI 1640 (11875119, Thermo Fisher Scientific) supplemented with 213 μg/mL ascorbic acid (A8960-5G, Sigma-Aldrich) and 500 μg/mL of bovine serum albumin (BSA) (A9418, Sigma-Aldrich); to this basal media, 3-4 μM of CHIR99021 was added prior to feeding. Precisely 48 hours later, the media was changed to the same basal medium supplemented with 2 μM WNT-C59 (S7037, Selleck Chemicals). On Day 4, the cells were fed only RBA media before transitioning to an RPMI 1640 + 1X B27™ plus insulin supplement (17504044, Thermo Fisher Scientific) basal medium from Day 6 to replating at Day 14.

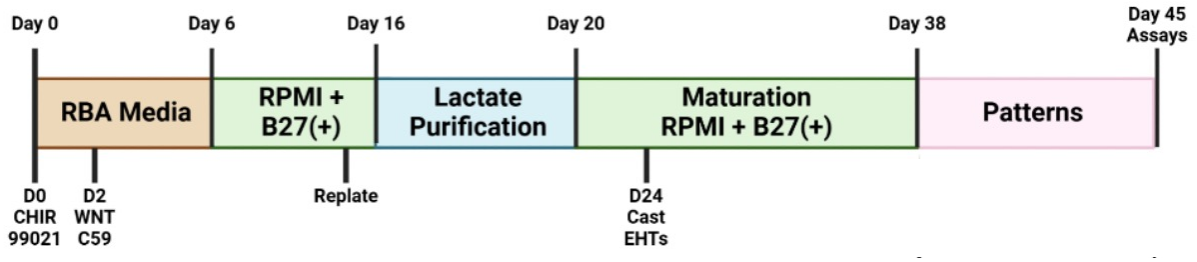

Figure 2.1. Protocol to generate and mature iPSC-CMs.

Our maturation protocol promotes the switch from the fetal α-MHC isoform to the adult β-MHC isoform through longer-term culture and 3D cues via extracellular matrix constructs (for EHTs) or patterned surfaces (for live cell imaging).

Replating consisted of selecting wells with >50% efficiency of cardiomyocyte differentiation, lifting the cells off the plate using 0.05% trypsin-EDTA (25300062, Fisher Scientific), and transferring them to Matrigel®-coated 6-well plates. Days 16 to 20 consisted of cardiomyocyte purification by leveraging previously described metabolic selection processes to starve fibroblasts (97). This involved feeding cells DMEM minus glucose (11966025, Thermo Fisher Scientific) with 4 mM sodium lactate (71718-10G, Sigma-Aldrich) for 4-6 days. Following this, cells were maintained in 6-well plates until used for EHT casting (Day 24) or micropatterning on polyacrylamide gels for live cell imaging (Day 38).

2.2.2 Casting engineered heart tissues

On Day 24, engineered heart tissues were cast in 24-well plates using as previously described (99). Briefly, hiPSC-CMs and HS27A cells (thawed one week prior) were lifted from plates using trypsin-EDTA. These cells were combined at a density of 500,000 cardiomyocytes and 50,000 HS27A cells in 87 µL of RPMI + B27 resuspension media and 10 µL of 50 mg/mL bovine fibrinogen (F8630-1G, Sigma-Aldrich) per tissue being cast. PDMS arrays were placed in a 24-well plate set with agar molds to hold the tissue suspension to prepare for cell suspension seeding.

To seed the cell suspension, 97 µL of the cell suspension and fibrinogen mixture was added to 3 µL of 100 U/mL bovine thrombin (T4648-1KU, Sigma-Aldrich), mixed gently, and added to the agar mold of each well. The casted tissues were then incubated at 37ºC for at least 80 minutes before being transferred to new 24-well plates with EHT maintenance media of RPMI + B27 + 5 g/L aminocaproic acid (A2504, Sigma-Aldrich). The tissues were maintained by being fed every other day until Day 45, when they were removed from the posts for assaying. In this assay, engineered heart tissues were removed from their posts, suspended between a lever arm and force transducer, and paced at 1 Hz on the Regnier Lab's IonOptix rig to derive twitch force and kinetic parameters such as time to peak force and time to baseline.

2.2.3 Micropatterning on polyacrylamide gels for live cell imaging

Creating micropatterned plates is a two- to three-day process modified from the myofibril assay patterning protocol (100) for use with a custom live cell imaging apparatus developed by the Yang Lab at the Institute for Stem Cell and Regenerative Medicine in Seattle, Washington. On the first day of this protocol, PDMS stamps with line patterns of 15 µm width and a 7:1 aspect ratio. Matrigel® 30X stock was diluted to a 5X concentration in DMEM/F-12 (11320033, Fisher Scientific) and added to the patterned surface of the stamps before being refrigerated for at least six hours at 4ºC or overnight.

The next step is making the polyacrylamide gels. 10 kPa gel precursors are formulated and degassed for at least 1 hour. 10 kPa is our chosen stiffness because it has been previously shown to best mimic physiological conditions in the heart and promote maturity (94). While precursors degassed, 25 mm glass coverslips were plasma-treated for 30 seconds and coated with 120 µL of bind-silane solution made by combining 3 µL of bind-silane (M6514, Sigma-Aldrich) with 950 µL 100% ethanol (04355223, Fisher Scientific) and 50 µL glacial acetic acid (14650391, Fisher

Scientific). After one minute, excess bind-silane was dabbed off and the coverslips were allowed to sit for 10 minutes, after which they were washed twice with 100% ethanol and allowed to dry and degas until further use.

Next, gels must be patterned and polymerized. To do this, the benchtop was set up with additional 25 mm coverslips rinsed in 100% ethanol and the stamps were retrieved from the fridge. The Matrigel® solution was then aspirated off of each stamp and just barely dried using a stream of air. Quickly, the dried stamp was flipped over onto a clean 25 mm coverslip and covered with a 50 g weight for five minutes. After five minutes, the weight was removed, and the stamp was allowed to sit for two additional minutes. To then create the gel, 0.5 µL of TEMED (1610800, Bio-Rad) and 5 µL of 10% w/v APS (1610700, Bio-Rad) was added to 1 mL of gel precursor and pipetted 150 µL at a time on each 25 mm bind-silane treated coverslip. Quickly, the 25 mm coverslip sandwiched against the PDMS stamp was detached and flipped face down onto the gel precursor to transfer the micropatterns. The gel was allowed to polymerize in the dark for 30 minutes before being covered in DPBS (14-190-250, Thermo Fisher Scientific) and stored at 4ºC overnight.

On the final day (1 week prior to Day 45 for the cells), cells were seeded on these patterns. Similar to other replating steps, cells were detached from 6-well plates using 0.05% trypsin-EDTA and resuspended in RPMI + 1X B27 + 10 µM ROCK inhibitor (Ri) (72308, Stemcell Technologies) at densities ranging from 50,000 to 300,000 cells per 400 µL. If cell suspensions were particularly gummy, bovine DNase I (260913, Sigma-Aldrich) was added, and the suspension was incubated for 10 minutes at 37ºC to homogenize the mixture. The polymerized gels were then removed from the fridge, and the coverslip not attached to the gel was removed with a razorblade and discarded. The gels were allowed to rehydrate in the incubator at 37ºC for 10 minutes before 400 µL of cell

suspension was gently seeded onto each gel. These gels were then allowed to sit in the incubator for 2-3 hours before being topped off with additional resuspension media.

The next day, the cells were fed RPMI + 1X B27. On Days 2, 4, and 6, cells were fed a 75:25 ratio of RPMI:DMEM minus glucose + 1X B27, which raises calcium concentration to improve contractility.

To image the cells, a coverslip was placed in a custom live cell imaging apparatus developed by the Yang Lab in Seattle, Washington. This system was hooked to a MyoPacer Cell Stimulator (IonOptix) delivering a 10 V, 10 ms bipolar pulse at a frequency of 1 Hz. The apparatus was placed in the Yokogawa CSU-W1 spinning disk confocal microscope (Nikon) in the Lynn and Mike Garvey Imaging Core at the Institute for Stem Cell and Regenerative Medicine (Seattle, Washington) and bathed in Tyrode's solution. A 40X Apo/LWD water immersion objective lens was used to capture nine-second videos of sarcomere shortening. Sarcomere shortening was analyzed in ImageJ/Fiji (NIH) using the BAR plugin by tracking distance between fluorescent Z disks in relaxed and contracted frames as previously described (101).

2.2.4 Statistics

EHT statistics were performed on biological replicates that had at least two technical replicates after outlier analysis was performed. A Welch's t-test was used in these experiments. Data are depicted as the average ± SEM.

For live cell imaging, average sarcomere shortening was captured for 1-2 myofibrils per cell and averaged to create technical replicates. A Welch's t-test was subsequently run on biological replicates. Data are depicted as the average ± SEM.

2.3 Results

2.3.1 Engineered heart tissues recapitulate the DCM phenotype without a change in kinetics

Isometric twitches were observed for a total of 14-22 technical replicates per genotype across five biological replicates. After outlier analysis and exclusion of any biological replicates with less than two technical replicates, the dataset comprised of $N = 3$ biological replicates with $n = 2$-4 technical replicates for WT and $N = 5$ biological replicates with $n = 2$-5 technical replicates for R369Q. The data are shown in **Fig. 2.2**.

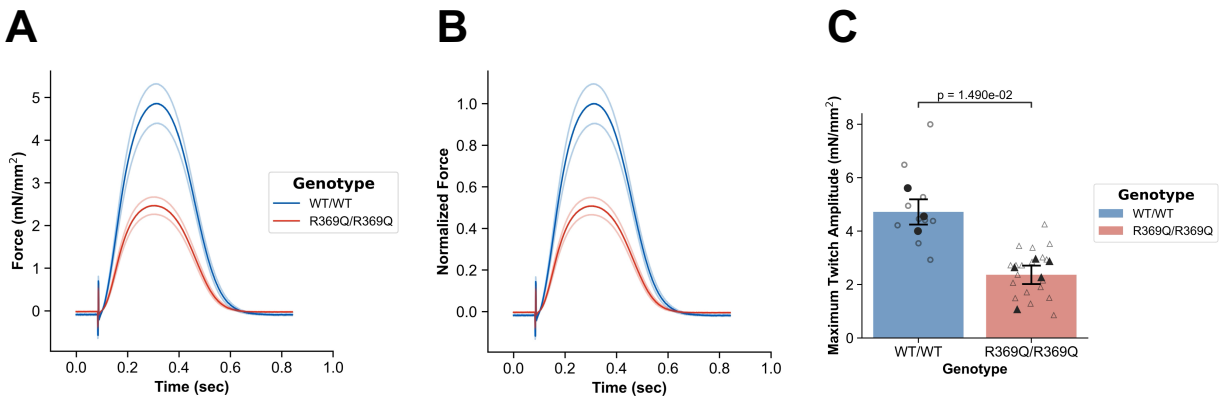

Figure 2.2. Twitch force is decreased in R369Q EHTs.
(**A** and **C**) Force is markedly reduced in mutant EHTs when comparing average traces. (**B**) By normalizing to peak WT force, we can see that the mutant can generate roughly 45-50% of the average maximum twitch force of the WT EHTs. (**C**) Quantifying average maximum twitch amplitude, we see there is a significant different in force generation capacity between WT and mutant. $N = 3$-5 per genotype, $n = 2$-5 per genotype per N, Welch's t-test.

The EHT rig also allows us to measure kinetic parameters such as the time to 50% and 90% of peak force generation as well as the time to 50% and 90% return to baseline from peak force generation. These data showed remarkably little variation across technical and biological replicates, indicating no observable change in EHT kinetics (**Fig. 2.3**).

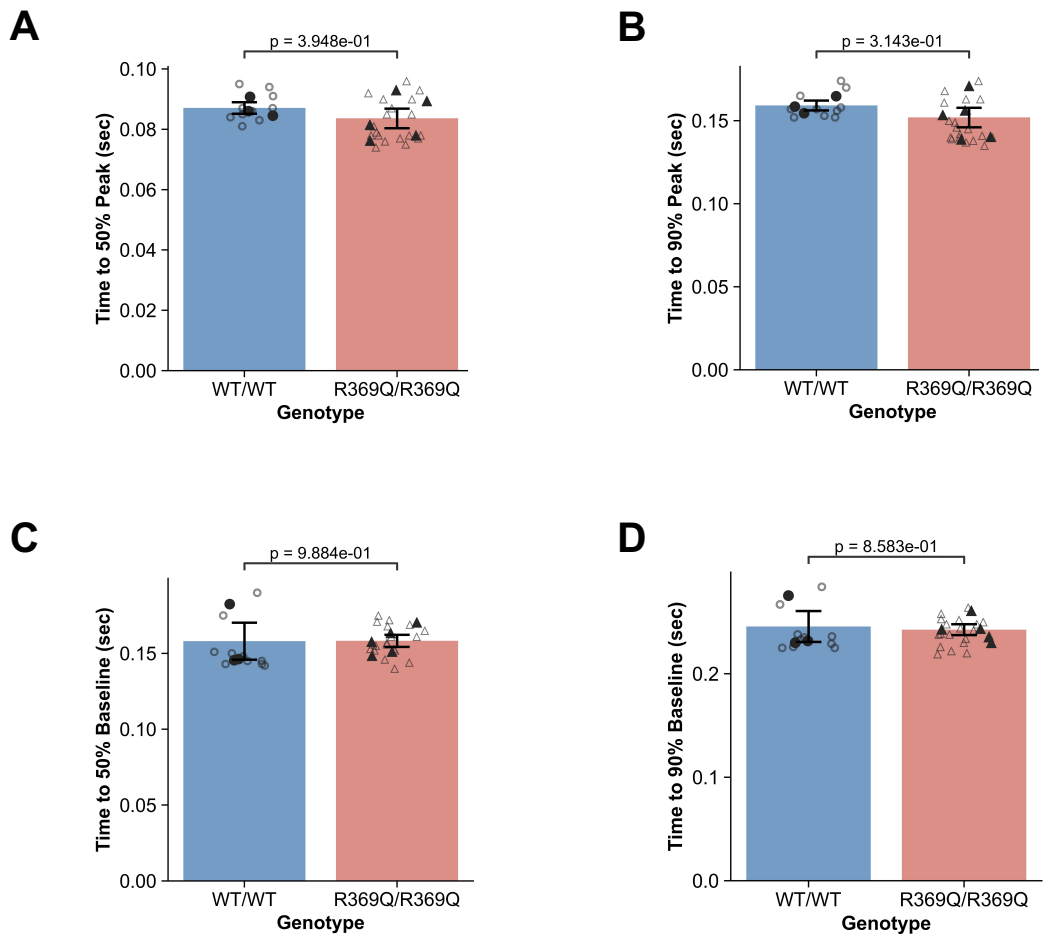

Figure 2.3. EHTs demonstrated no change in kinetic parameters.

Across all kinetic measurements (**A-D**), EHTs demonstrated no change in contractile parameters with notably small standards of error of the mean between technical replicates across several differentiations. *N* = 3-5 per genotype, *n* = 2-5 per genotype per *N*, Welch's t-test.

2.3.2 Live cell imaging data do not indicate any changes in average sarcomere shortening across genotypes

Live cell imaging analysis was performed for *N* = 3 biological replicates per genotype which contained *n* = 2-17 cells per biological replicate. Example contractile images (see **Fig. 2.4**) did demonstrate a notable decrease in distance between adjacent Z disks.

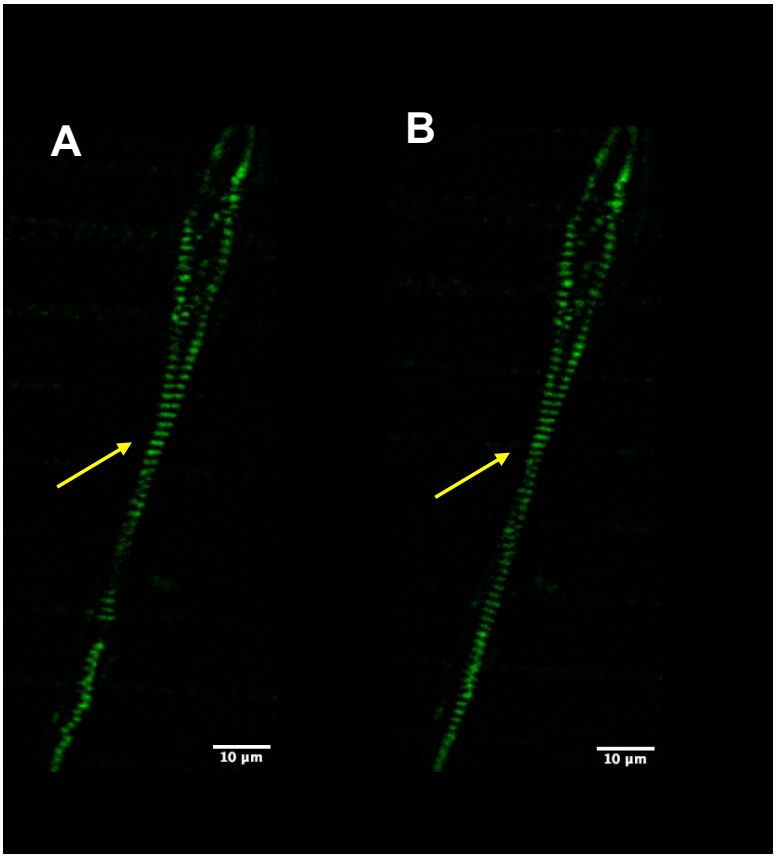

Figure 2.4. Representative images of a contracting cell.
The fiber analyzed in this cell (indicated by the yellow arrow) sees a marked decrease in distance between adjacent sarcomeres in a successive relaxed (**A**) and contracted (**B**) frame. By extracting the location of peak intensity values along the fiber, we can calculate the average change in distance between adjacent Z disks in relaxed versus contracted frames. For this WT cell, that value is 0.217 µm.

Cell-by-cell analysis across five differentiations yielded highly variable success with capturing high numbers of contracting cells, but three biological replicates of data encompassing at least two analyzable cells were collected. However, when these cells were analyzed fiber-by-fiber, no noticeable difference in average sarcomere shortening appeared (**Fig. 2.5**).

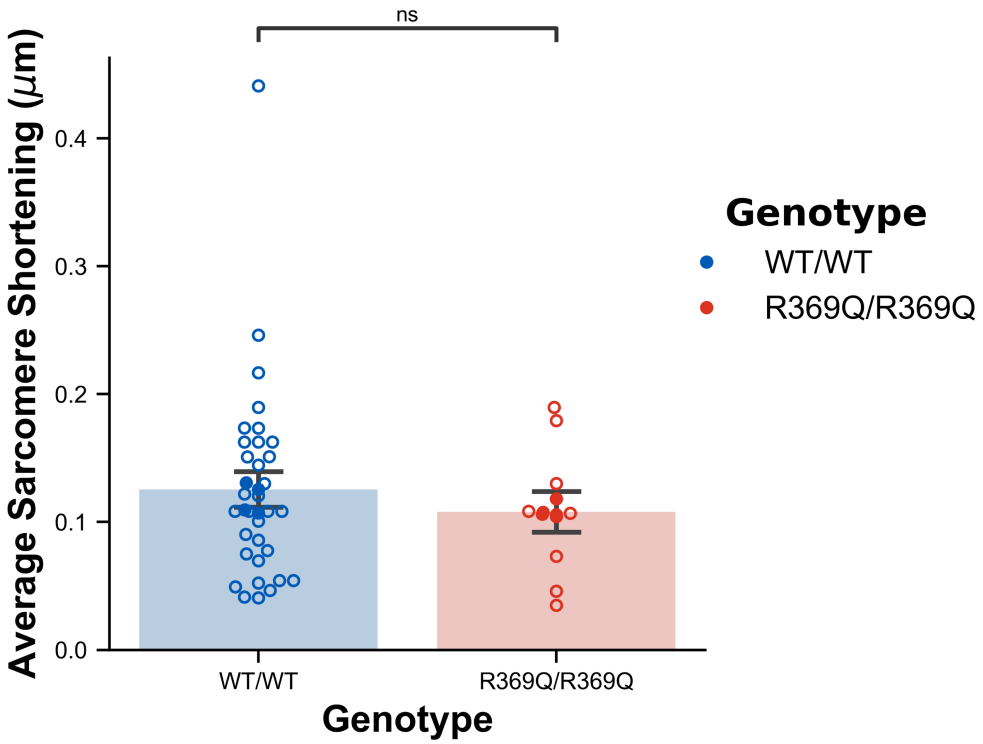

Figure 2.5. Live cell sarcomere shortening data showed no difference between WT and mutant. Across three separate biological replicates, there was no difference in average sarcomere shortening between WT and mutant with the standard error of the mean being very similar across both as well. Data may indicate a trend towards less sarcomere shortening in the mutant, which would support the DCM phenotype, but this experiment needs to be further powered to determine if this trend exists. N = 3 per genotype, n = 2-17 per genotype per N, Welch's t-test.

2.4 Discussion

The results of this aim provide evidence that the R369Q mutation does indeed decrease force generation capacity of the mutant tissues as well as suggesting a slight trend towards decreased sarcomere shortening in mutant cells. These results are encouraging as they demonstrate the power of our hiPSC-derived cardiomyocyte model as a platform to model "disease in a dish," but several outstanding questions remain.

2.4.1 Engineered heart tissues demonstrate the broader DCM phenotype but are difficult to standardize as a model system

As previously mentioned, engineered heart tissues are a powerful tool to study the effects of mutation in a system that matures cardiomyocytes with a 3D scaffold and accompanying extracellular cues (51,53). However, EHTs are often extremely heterogeneous, which can affect the ability of the researcher to see trends in force production and kinetics. As one example, Duong et al. have demonstrated that there is a significant different between the structural modulus of fibrinogen-thrombin hydrogels when fibrinogen concentration is held constant at 5 mg/mL while thrombin concentration increases from 2 U/mL to 5 U/mL (102). Our EHT constructs utilize a fibrinogen concentration of precisely 5 mg/mL and a thrombin concentration of 3 U/mL. As such, there is a question about the consistency of stiffness across EHTs when pipetting such small quantities of solution. Since the philosophy behind EHTs is to expose cells to a physiologically relevant set of external cues, significantly altering the stiffness of the hydrogel could impact contraction. Additionally, there are questions about how much the phenotype observed reflects differences in cell density across EHTs. Pipetting error when casting EHTs can lead to some EHTs with a notably smaller cross-sectional area than others. Moreover, this may not be exactly analogous to number of cells in the tissue contributing to force generation as other factors—including the mutation's effects on the cells—can lead to cell death at differential levels across a set of EHTs. As such, kinetic parameters derived from EHT experiments must be taken with a grain of salt and evaluated in the context of other studies such as immunohistochemistry of EHTs to determine cell counts across tissues.

2.4.2 Live cell imaging is a more granular model system than EHTs but still falls prey to the pitfalls of iPSC-derived systems

At first glance, live cell imaging seems to solve these issues as it does not require a hydrogel scaffold that can add confounding effects to the system. However, it is important to note that all whole-cell systems have distinct limitations in hiPSC-derived models. For instance, while our lab has demonstrated efficient conversion of α- to β-MHC in hiPSC-CMs, sarcomeric proteins are not the only components of muscle regulation that exhibit a fetal phenotype in stem cell models. Crucially, hiPSC-derived cardiomyocytes have immature calcium handling mechanisms, including a lack of T-tubules, low expression of the ryanodine (RYR) receptor and sarco/endoplasmic reticulum calcium ATPase (SERCA) pump, and dysregulated ionic currents—each of which impede efficient excitation-contraction (EC) coupling (103). hiPSC-CMs are also characterized by fewer myofibrils and higher myofibrillar disarray (103). Since this assay relies on tracking organized Z disks in myofibrils in an electrically paced rig, these differences can cause issues with data collection and analysis. For example, in the dataset presented here, the cells imaged were often in the minority as cells contracting at 1 Hz rather than beating spontaneously. Additionally, many cells were discarded in the analysis process as Z disk analysis proved impossible when myofibrils were poorly organized and Z disks were not clearly visible. Moreover, the experimental procedure can generate highly variable results. Ribeiro et al., the pioneers of this method, demonstrated that though a 7:1 aspect ratio of line patterns optimized the relationship between sarcomere shortening and force generation by increasing aligned myofibrils, there was still high variability in this relationship (see **Fig. 2.6**) (104). As such, the translation from the results presented here to definite conclusions about contractile regulation must be balanced with more

reductionist methods that eliminate some of the confounding variables in cell- and tissue-scale systems.

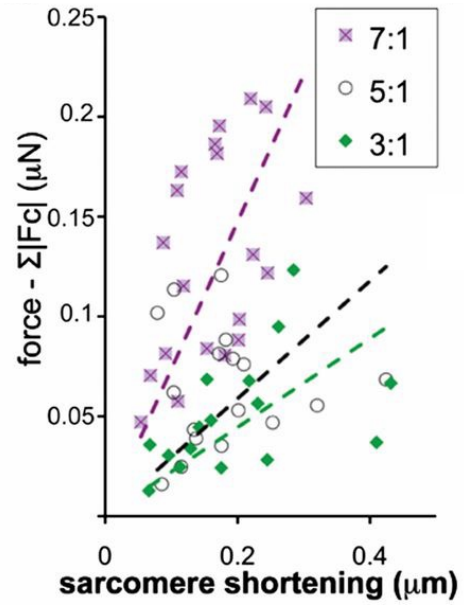

Figure 2.6. The relationship between sarcomere shortening and force generation is somewhat variable.

While the 7:1 aspect ratio greatly improves correlation between sarcomere shortening and force production, there is still some variability in the relationship between these two factors. While they may be a relatively linear scaling between sarcomere shortening and force generation when using a 7:1 aspect ratio, sarcomere shortening still does not fully account for differences in force generation. *Figure adapted from Figure 2 C of reference (104).*

2.5 Conclusions

Engineered heart tissues and cell imaging assays provide powerful models to interrogate changes in force generation on account of a highly controlled perturbation such as a mutation. The data presented here reveal that R369Q EHTs demonstrate a reduced force generation capacity at the tissue scale but an unclear phenotype at the cell scale. The heterogeneity in these results illustrates the need for a multiscale system to study contraction as there are benefits to both the larger and

smaller systems: with the larger, the model encompasses more of the complex elements of contraction, but with the smaller, the model eliminates some of the outstanding questions about other sources of variability in the system. Still, by taking our system down to the cell scale, we leave many questions about contractile regulation unanswered. While the larger scale systems presented in this aim do recapitulate the ultimate phenotype, we must utilize more granular methods of analysis to understand what specific components of cardiac muscle regulation are being impacted by R369Q. This is the focus of the second aim of this project.

Chapter 3

Understanding the Mechanistic Basis of R369Q's Contribution to a DCM Phenotype at a Subcellular Scale

3.1 Introduction

As previously mentioned, while cell- and tissue-scale models can provide insight into a mutation's impact on the entire array of processes involved in muscle contraction, they do not allow for measurement of distinct rates specific to different steps of muscle contraction nor the atomistic dynamics that could be compelling those changes.

In recent decades, expansion of muscle studies at the myofibril and molecular scale have greatly expanded the field's ability to pinpoint specific sites of dysregulation in systems perturbed by a mutation (105,106). The Regnier Lab in particular has a strong history of leveraging a custom myofibril rig to gather hiPSC-CM myofibril kinetics data and working at the cutting edge of computing to simulate protein dynamics, both of which can be used—individually or in tandem—to predict regulatory steps implicated in disease pathogenesis and the mechanisms of drug action (42,106). For instance, Steczina et al. used an elevated pool of ADP in submaximal calcium conditions to study the cardiac MyBP-C mutation c.772G > A (107). By considering the basic biochemical principle of product inhibition, it follows that if ADP release is accelerated by a mutation, then elevation of ADP in solution will more significantly attenuate relaxation kinetics,

which was indeed observed in the authors' experiments (107). In another study, Lee et al. integrated molecular dynamics studies of the hypertrophic cardiomyopathy-associated mutation G256E with myofibril mechanics to propose a mechanism of increased contractility due to slowed crossbridge detachment (demonstrated through myofibril mechanics) which may be borne out through disruptions in contacts in the transducer region (indicated in MD simulations) (106). Thus, a combination of organelle and molecular studies can refine hypotheses for the mechanism of contractile dysregulation.

In this same spirit, this aim presents a combination of experimental and computational work synthesized to better understand the R369Q mutation's contribution to the DCM phenotype elucidated in **Aim 1**. Taken together, these data provide strong support for the use of multiple modalities to interrogate disease development.

3.2 Methods

3.2.1 Differentiation of induced pluripotent stem cells into cardiomyocytes and subsequent maturation

Differentiation of hiPSCs into cardiomyocytes followed the same protocol listed in *Section 2.2.1* with no modifications.

3.2.2 Micropatterning on polyacrylamide gels for myofibril experiments

Patterning cells onto polyacrylamide gels followed an almost-identical procedure to the one listed in *Section 2.2.3*. The differences were as follows: 18 mm diameter glass-bottom 6-well plates and 18 mm top coverslips were used rather than 25 mm coverslips for plasma-treating and stamping the gel, and the smaller size of the glass well and coverslip required smaller volumes of bind silane

and gel precursor per gel (100 μL and 60 μL, respectively). Seeding densities and post-seeding feeding regimes were identical to those of the live cell imaging assay as well.

3.2.3 Myofibril assay

Myofibril kinetics experiments were performed according to previously established Regnier Lab protocols (100). First, hiPSC-CMs were skinned in a 1% Triton™ X-100 (AC327371000, Fisher Scientific) and myofibrils were collected from the gel surface using a cell scraper.

To perform the myofibril assay, a small amount of the myofibril solution described above was added to the custom myofibril rig (**Fig 3.1 A**) and a chosen myofibril was carefully suspended between a force transducer and motor arm and positioned above a double-barreled with one side containing high calcium activating solution and the other containing low calcium relaxing solution. The myofibril was rapidly switched between these two solutions to generate a force trace (**Fig 3.1 B-C**), which was subsequently normalized to myofibril cross sectional area before extracting rate constants for the rate of force development (k_{ACT}), rate and duration of the slow phase of relaxation ($k_{REL,slow}$ and $t_{REL,slow}$, respectively), and rate of the fast phase of relaxation ($k_{REL,fast}$). Experiments were performed with maximal (pCa 4.0) and submaximal (pCa 5.6) activating solutions.

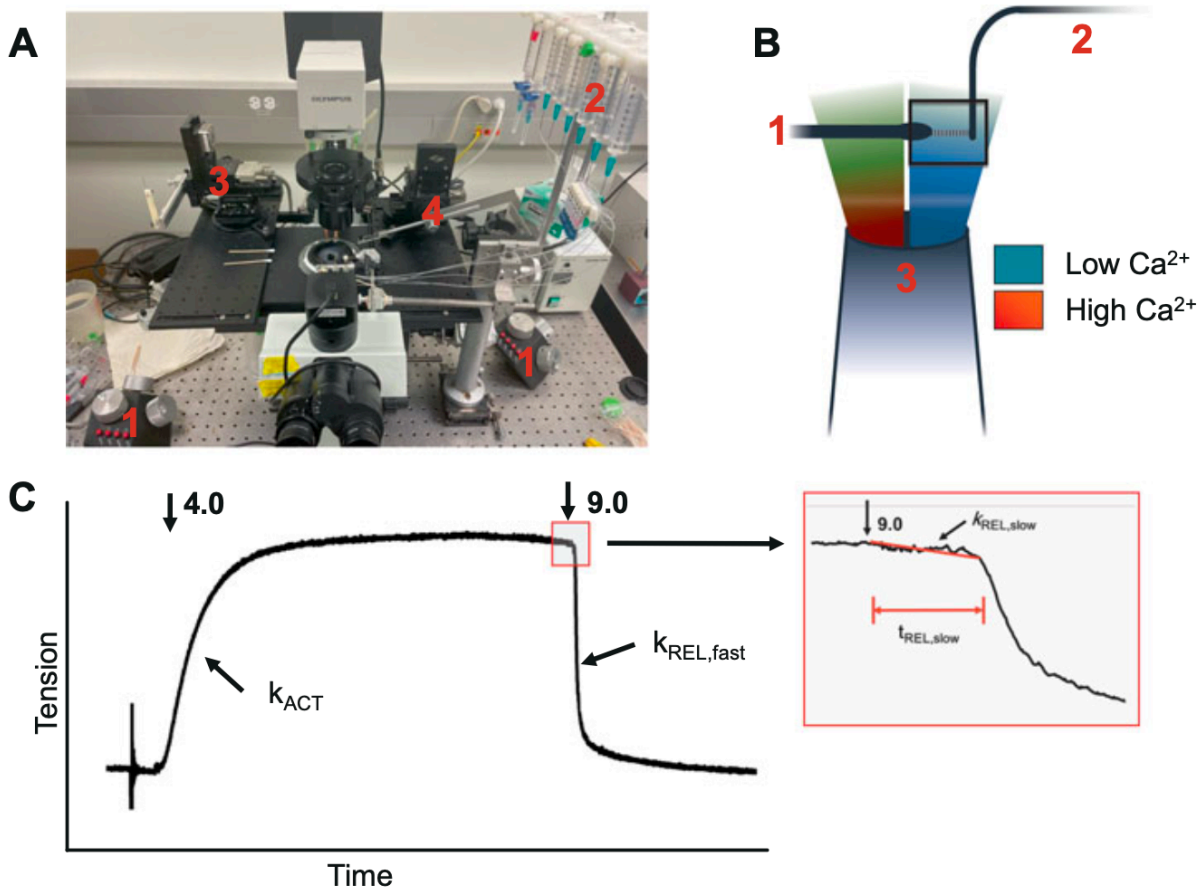

Figure 3.1. Set up of the myofibril assay.

In the myofibril assay, myofibrils are picked up on the myofibril rig (**A**) and rapidly switched between a low and high calcium solution while suspended between a motor arm and force transducer (**B**). This causes the myofibril to rapidly activate and relax, generating a curve (**C**) that can be used to analyze kinetic parameters. *Figure adapted from Figure 1 of reference (100).*

3.2.4 Molecular dynamics simulations

The foundation of the pre-powerstroke myosin model used in this study was the X-ray crystal structure of bovine β-MHC in complex with the essential light chain along with the drug omecamtiv mecarbil (OM), a vanadate ion, and other ligands (PDB: 5N69) (108). As per prior MD studies performed by our group (109), the model was adjusted to account for missing residues and to optimize loop geometry using *Modeller,* the vanadate ion was replaced with phosphate, and

unnecessary molecules such as water were removed (110). To generate an OM-free model, the OM ligand was also removed from the structure. This bovine template was used to homology model human β-MHC, which has high sequence similarity to bovine cardiac myosin.

Simulations were generated using AMBER20 with the ff14SB force field, TIP3P force field (for water), Li and Merz parameter set (for metal ion modeling), and GAFF2 force field (for ADP and phosphate) (111–118). The system underwent several steps of minimization before being equilibrated and subsequently simulated. Three simulations were performed per genotype that were 500 ns in length and had a granularity of 250 ps. Cα root mean square fluctuation (RMSF) and contact analyses were performed using *cpptraj* (119).

3.2.5 Statistics

For myofibril experiments, there were N = 12-13 biological replicates per genotype with n = 2-6 technical replicates per N at pCa 4.0. At pCa 5.6, there were N = 6-8 biological replicates per genotype with n = 2-6 technical replicates per N. Outlier analysis was performed, and two WT differentiations were removed across all parameters, leaving the biological replicate count at N = 11-12 and N = 6 per genotype for pCa 4.0 and 5.6, respectively. Welch's t-test was performed on biological replicates and data are depicted as the average ± SEM.

MD contact analysis data show statistically significant contacts across the three simulations with a Student's t-test and difference in average percentage contact time >10%.

3.3 Results

3.3.1 Myofibril experiments indicate a depression in force generation, no change in activation kinetics, and accelerated relaxation kinetics

Data were successfully collected at pCa 4.0 for 11-12 replicates, which revealed a strong decrease in force generation by mutant myofibrils, which appeared to generate only 40% of the force WT (**Fig. 3.2 A**). Additional measurements at the more physiologically relevant pCa 5.6 demonstrated that this decrease in force was statistically significant at both calcium concentrations (**Fig. 3.2 B**).

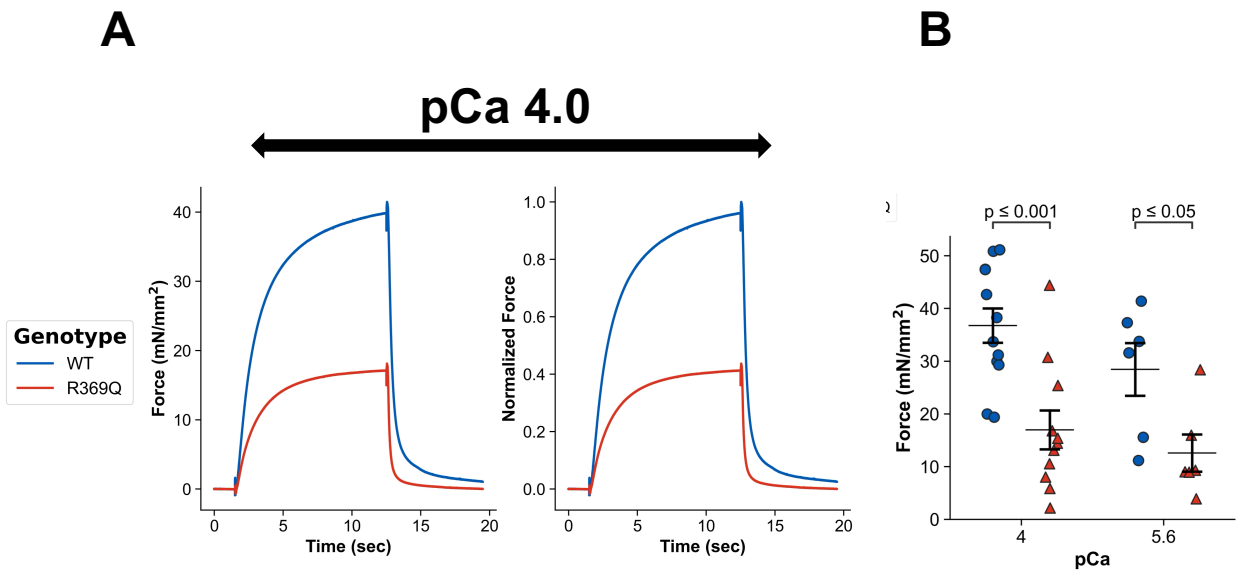

Figure 3.2. Force results from the myofibril assay.
R369Q (red) average traces at pCa 4.0 demonstrate that the mutant produces less than half as much force as the WT myofibrils (blue) (**A**). This phenomenon of decreased force recapitulates the DCM phenotype and is also present at submaximal calcium of pCa 5.6 (**B**).

Next, we examined the kinetics parameters extracted from the myofibril assay. Analysis across maximal and submaximal calcium revealed significantly faster relaxation kinetics in both the slow

and fast phase while activation kinetics demonstrated no change at pCa 4.0 and a slight increase at pCa 5.6 (**Fig. 3.3**).

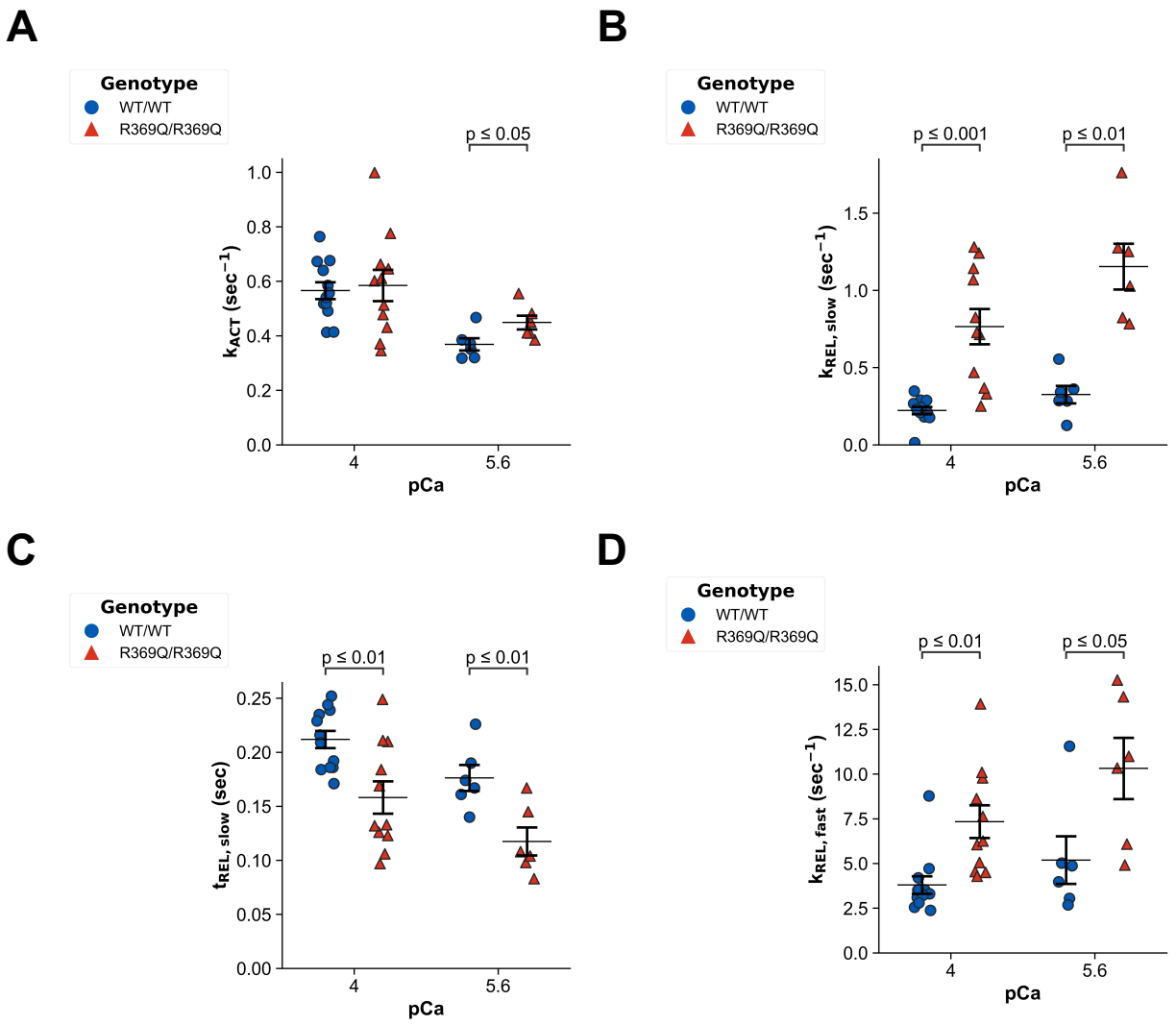

Figure 3.3. Changes in kinetic parameters in the myofibril assay.

Activation kinetics were not significantly different between WT and mutant myofibrils at pCa 4.0 and were slightly, but significantly, increased at pCa 5.6 (**A**). Meanwhile, the slow phase of relaxation appears to be much faster in the mutant with a higher average $k_{REL,slow}$ and shorter $t_{REL,slow}$ in R369Q myofibrils (**B**-**C**). The fast phase of relaxation is also notably faster in the mutant at both calcium concentrations (**D**).

3.3.2 Molecular dynamics simulations of the pre-powerstroke state show increased flexibility in the mutant, particularly in loop 2

To first understand general differences in protein dynamics, we performed a root mean square fluctuation (RMSF) analysis, which calculates the flexibility of each residue within the protein structure. Comparing average RMSF per residue in wild type simulations to mutant simulations, it became apparent that the mutant structures were on average globally more flexible than the wild type structures (see **Fig. 3.4 A**). Still, some regions of the RMSF plot illustrated drastic differences in flexibility between the average wild type and R369Q simulation. Most notably, the loop 2 structure of myosin is much more promiscuous in mutant simulations. An analysis of loop 2 dynamics over the course of representative 500 ns WT and R369Q simulations revealed that loop 2 sequestered against the bulk of the motor domain in the WT simulation but remained very labile in the R369Q mutation (**Fig. 3.4 B**).

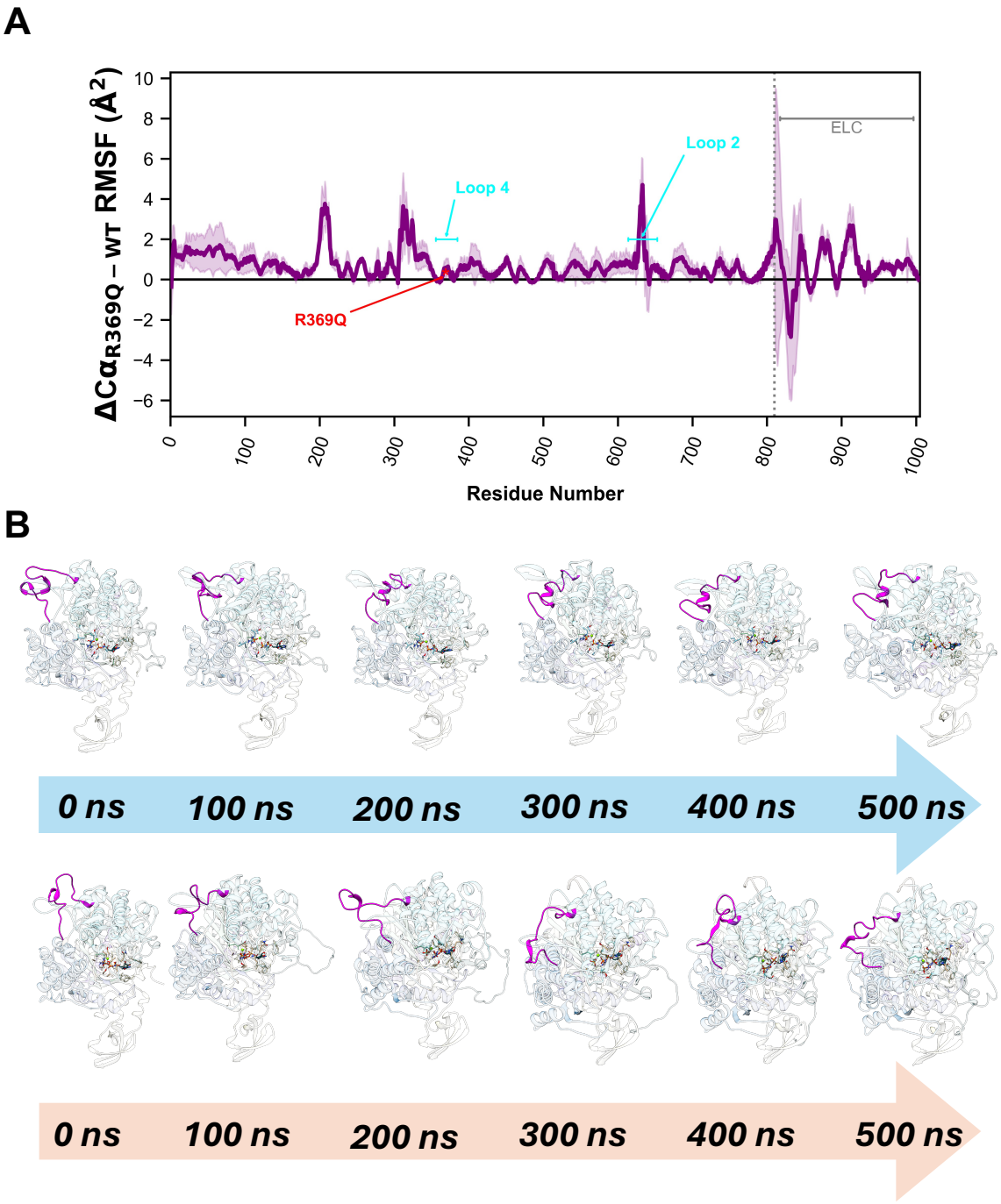

Figure 3.4. Loop 2 is a particularly flexible domain of mutant pre-powerstroke myosin as compared to the wild type.

(**A**) While a difference plot shows that R369Q simulations are more flexible across the whole structure than WT simulations, loop 2 flexibility is particularly different across genotypes. (**B**) Time series plots of WT (blue) and mutant (orange) structures show that loop 2 (magenta) sequesters against the S1 head in the WT

simulation after approximately 200 ns but continues to sample diverse conformations in the R369Q simulation.

3.3.3 Contacts between switch I and the upper 50 kDa domain are disrupted in mutant simulations

Reflecting back on the RMSF analysis, another location of increased flexibility in mutant simulations is in residues 300-340, which encompass parts of the upper 50 kDa domain. Close examinations of MD simulations revealed a potential change in contacts between switch I—a structure known to be important for nucleotide-binding pocket coordination—and the upper 50 kDa domain. In multiple mutant simulations, a flexible loop in the upper 50 kDa domain was seen to peel up and away from switch I, potentially disrupting interactions between the actin-binding cleft and the nucleotide-binding pocket (**Fig. 3.5**).

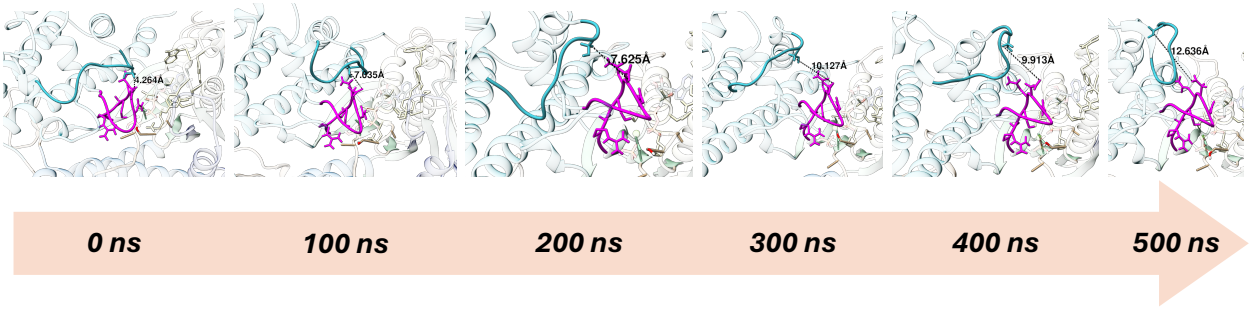

Figure 3.5. Switch I contacts with the upper 50 kDa domain are disrupted in R369Q simulations.
A time series plot of evolving interactions between switch I (magenta) and a flexible loop in the upper 50 kDa domain (teal) demonstrate a gradual increase in distance between the two structures as the loop in the upper 50 kDa peels away from switch I.

To quantify this change, we performed quantitative contact analysis using *cpptraj* for residues interacting with switch I (residues 232-244). Quantification showed significant decreases in many

contacts between switch I and the upper 50 kDa domain, with some average contact times decreasing by over 50% from WT simulations to mutant simulations (**Fig. 3.6**).

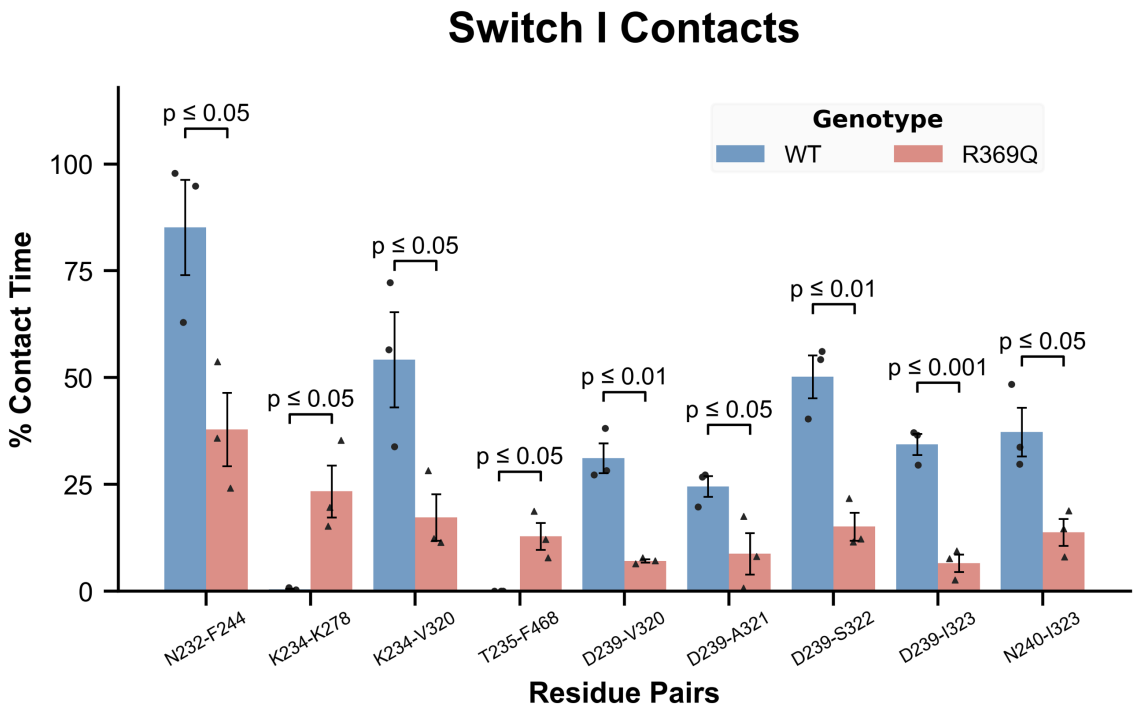

Figure 3.6. Switch I loses significant contact time with residues in the upper 50 kDa domain. Switch I residues (232-244, listed first in residue pairs) show global decreases in contact time with residues in a flexible loop in the upper 50 kDa domain (residues 320-323). This could result in loss of structural signal communication from the actin-binding cleft to the nucleotide binding pocket, which could be crucial in modulating the weak-to-strong actomyosin complex transition.

3.4 Discussion

Given prior steered MD results demonstrating a role for R369 in activating the thin filament by translocating tropomyosin, we expected to see a decrease in activation kinetics to reflect the increased barrier to thin filament activation when the positive R369 is mutated to a polar Q369. However, we interestingly did not observe a change in activation kinetics between genotypes at

maximal calcium and even saw a slight increase in activation kinetics for the mutant at submaximal calcium, reflecting little to no change in activation kinetics.

The results presented here can be explained in the context of the electrostatic repulsion mechanism proposed by Rynkiewicz et al. if activation results in conjunction with relaxation kinetics. R369Q myofibrils demonstrated a substantial and significant increase in the rate of relaxation, meaning crossbridges take less time to detach from actin and the thin filament is quicker to deactivate. Just as charge-charge repulsion can contort tropomyosin into the M-state, abolishing some of that repulsion through a charge change could make it easier for tropomyosin to snap back from the energetically unfavorable M state to the more stable C state, thus facilitating faster crossbridge detachment (120). Decreased numbers of attached crossbridges at any given time due to this rapid off-rate could decrease the force generation capacity of R369Q myofibrils.

The pre-powerstroke MD studies provide further evidence that R369Q modulates thin filament interactions. We chose to model the pre-powerstroke state because it is the biochemical state primed to make initial contact with actin. Prior structural studies have indicated a role for loop 2 in actin-sensing and the initial electrostatic interactions that govern the weak actomyosin complex (66,121). Thus, increased flexibility of loop 2 might impede actomyosin complexing or hinder isomerization to the strongly bound state, further decreasing the number of force-producing, cycling myosin heads. Additionally, switch I has been demonstrated to be important in MgADP coordination and ADP release (66). Thus, a disruption in contacts involving switch I could modulate the process of ADP release, which is the rate-limiting step of the crossbridge cycle and encompassed in the myofibril parameter $k_{REL,slow}$.

These results provide a strong basis for a mechanism by which R369Q dysregulates normal cardiac contraction and serve as a blueprint for additional experiments to further dissect disease

pathogenesis. For example, stopped flow fluorometric measurements to measure the rate of ADP release from an actin•S1 complex could further assess how ADP release rates are altered with the R369Q mutation (122).

3.5 Conclusions

While cell- and tissue-scale assays can be useful for characterizing the larger-scale phenotypic effects of a pathogenic mutation, they struggle to provide the level of control needed to interrogate specific molecular mechanisms of disease pathogenesis that can be leveraged for discovery of novel therapeutics. By contrast, myofibril mechanics and MD simulations offer highly tunable systems in which researchers can precisely control many of the confounding factors found in cell and tissue systems. In myofibril assays, isolating the contractile organelles and activating them with calcium solutions eliminates the effects that calcium handling mechanisms involved in EC coupling could have on contractile regulation, allowing the effects of the mutation on sarcomeric proteins to speak for themselves. MD models offer even more precision as they allow us to study contractile systems at an atomistic scale and generate highly specific hypotheses than can be further probed experimentally. Thus, subcellular and molecular approaches are essential complements to cell and tissue experimental workflows in order to develop the most comprehensive understanding of how a single point mutation can ultimately result in severe disease.

Chapter 4

Conclusions and Future Directions

4.1 Summary of work to date

The work presented here leverages a multiscale approach to study the mechanistic basis for the R369Q myosin mutation's contribution to a dilated cardiomyopathy phenotype. Beginning at the largest scale, we saw that engineered heart tissues did indeed have significantly reduced force generation capacity and a slight trend towards reduced sarcomere shortening in live cell imaging analysis. Because this higher level of structure introduces several confounding variables into our system, we also leveraged the subcellular myofibril mechanics assay and molecular dynamics simulations to connect the phenotypic results observed in EHTs and cells to a potential mechanism underpinning these pathogenic characteristics. Myofibril kinetics assays demonstrated a dramatic increase in relaxation kinetics, indicating faster crossbridge detachment and possible acceleration of ADP release. This is further supported by MD simulations which show switch I, important for ADP coordination and release, has significantly altered contacts with neighboring residues in mutant simulations. Thin filament interactions could also be impacted by a highly flexible and promiscuous loop 2 in R369Q simulations, which could impair initial actomyosin binding. These effects taken together with prior steered MD results suggesting a role for R369 in thin filament activation point to a multi-tiered effect on crossbridge cycling and cooperativity that ultimately lead to the DCM phenotype.

4.2 Outstanding questions and future directions

4.2.1 Sarcomeric protein isoforms and impacts on contraction

As previously mentioned, one limitation of hiPSC-CMs is their display of a fetal phenotype (103). While our group has developed methods to achieve near-complete conversion from α- to β-myosin, other sarcomeric proteins have fetal isoforms not specifically targeted in our maturation protocol. For example, one study found that embryonic stem cell-derived cardiomyocytes had significant populations of slow skeletal TnI and TnT while adult cardiomyocytes only contain the cardiac isoforms of TnI and TnT (123). Similarly, stem cell-derived cardiomyocytes contain a mixture of α, β, and κ isoforms of tropomyosin while adult cardiomyocytes primarily contain α-tropomyosin (123). Modulation of the troponin complex and tropomyosin filament through presence of different isoform ratios detracts from faithful recapitulation of adult cardiac function and must be addressed to truly isolate the effect of the R369Q mutation on contractile regulation. Western blots will be performed in the future to assess the isoform distribution of thin filament proteins.

4.2.2 The role of phosphorylation in contractile regulation

Several sarcomeric proteins can modulate contraction through phosphorylation sites. For example, phosphorylated cMyBP-C has been demonstrated to increase crossbridge formation while phosphorylation of cTnI and cTnT increase the rate of relaxation and decrease calcium sensitivity (124). Thus, Phos-tag gels must be run for these specific proteins to check whether differences in phosphorylation may play a role in the different contractile phenotypes across wild type and R369Q.

REFERENCES

1. Bozkurt B, Coats AJS, Tsutsui H, Abdelhamid CM, Adamopoulos S, Albert N, et al. Universal definition and classification of heart failure: a report of the Heart Failure Society of America, Heart Failure Association of the European Society of Cardiology, Japanese Heart Failure Society and Writing Committee of the Universal Definition of Heart Failure. Eur J Heart Fail. 2021;23(3):352–80.

2. Chapter 1: The Burden of Heart Failure. Am J Med. 2024 Feb 1;137(2):S3–8.

3. Martin SS, Aday AW, Allen NB, Almarzooq ZI, Anderson CAM, Arora P, et al. 2025 Heart Disease and Stroke Statistics: A Report of US and Global Data From the American Heart Association. Circulation. 2025 Feb 25;151(8):e41–660.

4. Weintraub RG, Semsarian C, Macdonald P. Dilated cardiomyopathy. The Lancet. 2017 Jul 22;390(10092):400–14.

5. Rosenbaum AN, Agre KE, Pereira NL. Genetics of dilated cardiomyopathy: practical implications for heart failure management. Nat Rev Cardiol. 2020 May;17(5):286–97.

6. Reichart D, Magnussen C, Zeller T, Blankenberg S. Dilated cardiomyopathy: from epidemiologic to genetic phenotypes. J Intern Med. 2019;286(4):362–72.

7. Merlo M, Caiffa T, Gobbo M, Adamo L, Sinagra G. Reverse remodeling in Dilated Cardiomyopathy: Insights and future perspectives. IJC Heart Vasc. 2018 Mar 1;18:52–7.

8. Lakdawala NK, Winterfield JR, Funke BH. Dilated Cardiomyopathy. Circ Arrhythm Electrophysiol. 2013 Feb;6(1):228–37.

9. Hofmeyer M, Haas GJ, Jordan E, Cao J, Kransdorf E, Ewald GA, et al. Rare Variant Genetics and Dilated Cardiomyopathy Severity: The DCM Precision Medicine Study. Circulation. 2023 Sep 12;148(11):872–81.

10. Escobar-Lopez L, Ochoa JP, Mirelis JG, Espinosa MÁ, Navarro M, Gallego -Delgado María, et al. Association of Genetic Variants With Outcomes in Patients With Nonischemic Dilated Cardiomyopathy. JACC. 2021 Oct 26;78(17):1682–99.

11. Jansen M, de Brouwer R, Hassanzada F, Schoemaker AE, Schmidt AF, Kooijman-Reumerman MD, et al. Penetrance and Prognosis of *MYH7* Variant-Associated Cardiomyopathies. JACC Heart Fail. 2024 Jan 1;12(1):134–47.

12. Newman NA, Burke MA. Dilated Cardiomyopathy: A Genetic Journey from Past to Future. Int J Mol Sci. 2024 Jan;25(21):11460.

13. Seidel F, Holtgrewe M, Al-Wakeel-Marquard N, Opgen-Rhein B, Dartsch J, Herbst C, et al. Pathogenic Variants Associated With Dilated Cardiomyopathy Predict Outcome in Pediatric Myocarditis. Circ Genomic Precis Med. 2021 Aug;14(4):e003250.

14. Seidman JG, Seidman C. The Genetic Basis for Cardiomyopathy: from Mutation Identification to Mechanistic Paradigms. Cell. 2001 Feb 23;104(4):557–67.

15. Burkett EL, Hershberger RE. Clinical and genetic issues in familial dilated cardiomyopathy. J Am Coll Cardiol. 2005 Apr 5;45(7):969–81.

16. Dellefave L, McNally EM. The genetics of dilated cardiomyopathy. Curr Opin Cardiol. 2010 May;25(3):198–204.

17. Merlo M, Sinagra G, Carniel E, Slavov D, Zhu X, Barbati G, et al. Poor Prognosis of Rare Sarcomeric Gene Variants in Patients with Dilated Cardiomyopathy. Clin Transl Sci. 2013;6(6):424–8.

18. Rampersaud E, Siegfried JD, Norton N, Li D, Martin E, Hershberger RE. Rare variant mutations identified in pediatric patients with dilated cardiomyopathy. Prog Pediatr Cardiol. 2011 Jan 1;31(1):39–47.

19. de Frutos F, Ochoa JP, Navarro -Peñalver Marina, Baas A, Bjerre JV, Zorio E, et al. Natural History of MYH7-Related Dilated Cardiomyopathy. JACC. 2022 Oct 11;80(15):1447–61.

20. Whayne TF. Clinical Use of Digitalis: A State of the Art Review. Am J Cardiovasc Drugs. 2018 Dec 1;18(6):427–40.

21. Casu G, Merella P. Diuretic Therapy in Heart Failure – Current Approaches. Eur Cardiol Rev. 2015 Jul;10(1):42–7.

22. Sacks CA, Jarcho JA, Curfman GD. Paradigm Shifts in Heart-Failure Therapy — A Timeline. N Engl J Med. 2014 Sep 11;371(11):989–91.

23. Weldy CS, Ashley EA. Towards precision medicine in heart failure. Nat Rev Cardiol. 2021 Nov;18(11):745–62.

24. Cojan-Minzat BO, Zlibut A, Agoston-Coldea L. Non-ischemic dilated cardiomyopathy and cardiac fibrosis. Heart Fail Rev. 2021 Sep 1;26(5):1081–101.

25. The SOLVD Investigators. Effects of Enalapril on Mortality in Severe Congestive Heart Failure. N Engl J Med. 1987 Jun 4;316(23):1429–35.

26. The SOLVD Investigators. Effect of Enalapril on Survival in Patients with Reduced Left Ventricular Ejection Fractions and Congestive Heart Failure. N Engl J Med. 1991 Aug 1;325(5):293–302.

27. McMurray JJV, Packer M, Desai AS, Gong J, Lefkowitz MP, Rizkala AR, et al. Angiotensin–Neprilysin Inhibition versus Enalapril in Heart Failure. N Engl J Med. 2014 Sep 11;371(11):993–1004.

28. CIBIS-II Investigators and Committees. The Cardiac Insufficiency Bisoprolol Study II (CIBIS-II): a randomised trial. The Lancet. 1999 Jan 2;353(9146):9–13.

29. MERIT-HF Study Group. Effect of metoprolol CR/XL in chronic heart failure: Metoprolol CR/XL Randomised Intervention Trial in-Congestive Heart Failure (MERIT-HF). The Lancet. 1999 Jun 12;353(9169):2001–7.

30. Packer M, Coats AJS, Fowler MB, Katus HA, Krum H, Mohacsi P, et al. Effect of Carvedilol on Survival in Severe Chronic Heart Failure. N Engl J Med. 2001 May 31;344(22):1651–8.

31. Oliver E, Mayor Jr F, D'Ocon P. Beta-blockers: Historical Perspective and Mechanisms of Action. Span J Cardiol. 2019 Jun 6;72(10):853–62.

32. Pitt B, Zannad F, Remme WJ, Cody R, Castaigne A, Perez A, et al. The Effect of Spironolactone on Morbidity and Mortality in Patients with Severe Heart Failure. N Engl J Med. 1999 Sep 2;341(10):709–17.

33. Rogers JK, McMurray JJV, Pocock SJ, Zannad F, Krum H, van Veldhuisen DJ, et al. Eplerenone in Patients With Systolic Heart Failure and Mild Symptoms. Circulation. 2012 Nov 6;126(19):2317–23.

34. Ponikowski P, Voors AA, Anker SD, Bueno H, Cleland JGF, Coats AJS, et al. 2016 ESC Guidelines for the diagnosis and treatment of acute and chronic heart failure. Eur J Heart Fail. 2016;18(8):891–975.

35. Bristow MR, Saxon LA, Boehmer J, Krueger S, Kass DA, De Marco T, et al. Cardiac-Resynchronization Therapy with or without an Implantable Defibrillator in Advanced Chronic Heart Failure. N Engl J Med. 2004 May 20;350(21):2140–50.

36. Cleland JGF, Daubert JC, Erdmann E, Freemantle N, Gras D, Kappenberger L, et al. The Effect of Cardiac Resynchronization on Morbidity and Mortality in Heart Failure. N Engl J Med. 2005 Apr 14;352(15):1539–49.

37. Køber L, Thune JJ, Nielsen JC, Haarbo J, Videbæk L, Korup E, et al. Defibrillator Implantation in Patients with Nonischemic Systolic Heart Failure. N Engl J Med. 2016 Sep 29;375(13):1221–30.

38. Rose EA, Gelijns AC, Moskowitz AJ, Heitjan DF, Stevenson LW, Dembitsky W, et al. Long-Term Use of a Left Ventricular Assist Device for End-Stage Heart Failure. N Engl J Med. 2001 Nov 15;345(20):1435–43.

39. Recchia FA, Lionetti V. Animal Models of Dilated Cardiomyopathy for Translational Research. Vet Res Commun. 2007 Aug 1;31(1):35–41.

40. Ponzoni M, Coles JG, Maynes JT. Rodent Models of Dilated Cardiomyopathy and Heart Failure for Translational Investigations and Therapeutic Discovery. Int J Mol Sci. 2023 Jan;24(4):3162.

41. Marcello M, Cetrangolo V, Savarese M, Udd B. Use of animal models to understand titin physiology and pathology. J Cell Mol Med. 2022;26(20):5103–12.

42. Kooiker KB, Mohran S, Turner KL, Ma W, Martinson A, Flint G, et al. Danicamtiv Increases Myosin Recruitment and Alters Cross-Bridge Cycling in Cardiac Muscle. Circ Res. 2023 Aug 18;133(5):430–43.

43. Sewanan LR, Campbell SG. Modelling sarcomeric cardiomyopathies with human cardiomyocytes derived from induced pluripotent stem cells. J Physiol. 2020;598(14):2909–22.

44. Smith AST, Macadangdang J, Leung W, Laflamme MA, Kim DH. Human iPSC-derived cardiomyocytes and tissue engineering strategies for disease modeling and drug screening. Biotechnol Adv. 2017 Jan 1;35(1):77–94.

45. Sallam K, Kodo K, Wu JC. Modeling Inherited Cardiac Disorders: a Cell is Worth a Thousand Genes. Circ J Off J Jpn Circ Soc. 2014;78(4):784–94.

46. Sun N, Yazawa M, Liu J, Han L, Sanchez-Freire V, Abilez OJ, et al. Patient-Specific Induced Pluripotent Stem Cells as a Model for Familial Dilated Cardiomyopathy. Sci Transl Med. 2012 Apr 18;4(130):130ra47-130ra47.

47. Tse HF, Ho JCY, Choi SW, Lee YK, Butler AW, Ng KM, et al. Patient-specific induced-pluripotent stem cells-derived cardiomyocytes recapitulate the pathogenic phenotypes of dilated cardiomyopathy due to a novel DES mutation identified by whole exome sequencing. Hum Mol Genet. 2013 Apr 1;22(7):1395–403.

48. Siu CW, Lee YK, Ho JCY, Lai WH, Chan YC, Ng KM, et al. Modeling of lamin A/C mutation premature cardiac aging using patient-specific induced pluripotent stem cells. Aging. 2012 Dec 3;4(11):803–22.

49. Ganipineni VDP, Gutlapalli SD, Danda S, Garlapati SKP, Fabian D, Okorie I, et al. Clustered Regularly Interspaced Short Palindromic Repeats (CRISPR) in Cardiovascular Disease: A Comprehensive Clinical Review on Dilated Cardiomyopathy. Cureus. 2023 Mar 5;15(3):e35774.

50. Nguyen Q, Lim KRQ, Yokota T. Genome Editing for the Understanding and Treatment of Inherited Cardiomyopathies. Int J Mol Sci. 2020 Jan;21(3):733.

51. Hoes MF, Bomer N, Meer P. Concise Review: The Current State of Human In Vitro Cardiac Disease Modeling: A Focus on Gene Editing and Tissue Engineering. Stem Cells Transl Med. 2019 Jan 1;8(1):66–74.

52. Marchianò S, Bertero A, Murry CE. Learn from your elders: developmental biology lessons to guide maturation of stem cell-derived cardiomyocytes. Pediatr Cardiol. 2019 Oct;40(7):1367–87.

53. Tu C, Chao BS, Wu JC. Strategies for Improving the Maturity of Human Induced Pluripotent Stem Cell-Derived Cardiomyocytes. Circ Res. 2018 Aug 17;123(5):512–4.

54. Tani H, Tohyama S. Human Engineered Heart Tissue Models for Disease Modeling and Drug Discovery. Front Cell Dev Biol [Internet]. 2022 Mar 31 [cited 2024 Mar 14];10. Available from: https://www.frontiersin.org/articles/10.3389/fcell.2022.855763

55. Camman M, Joanne P, Agbulut O, Hélary C. 3D models of dilated cardiomyopathy: Shaping the chemical, physical and topographical properties of biomaterials to mimic the cardiac extracellular matrix. Bioact Mater. 2022 Jan 1;7:275–91.

56. Seguret M, Vermersch E, Jouve C, Hulot JS. Cardiac Organoids to Model and Heal Heart Failure and Cardiomyopathies. Biomedicines. 2021 May;9(5):563.

57. Ito M, Nomura S, Morita H, Komuro I. Trends and Limitations in the Assessment of the Contractile Properties of Human Induced Pluripotent Stem Cell-Derived Cardiomyocytes From Patients With Dilated Cardiomyopathy. Front Cardiovasc Med [Internet]. 2020 Sep 3 [cited 2024 Mar 14];7. Available from: https://www.frontiersin.org/articles/10.3389/fcvm.2020.00154

58. Harris D, editor. Mohrman and Heller's Cardiovascular Physiology. 10th ed. McGraw Hill; 2023.

59. Hollingsworth SA, Dror RO. Molecular Dynamics Simulation for All. Neuron. 2018 Sep 19;99(6):1129–43.

60. Kawakubo T, Okada O, Minami T. Dynamic conformational changes due to the ATP hydrolysis in the motor domain of myosin: 10-ns molecular dynamics simulations. Biophys Chem. 2009 Apr 1;141(1):75–86.

61. Matyushenko AM, Koubassova NA, Shchepkin DV, Kopylova GV, Nabiev SR, Nikitina LV, et al. The effects of cardiomyopathy-associated mutations in the head-to-tail overlap junction of α-tropomyosin on its properties and interaction with actin. Int J Biol Macromol. 2019 Mar 15;125:1266–74.

62. Racca AW, Rynkiewicz MJ, LaFave N, Ghosh A, Lehman W, Moore JR. M8R tropomyosin mutation disrupts actin binding and filament regulation: The beginning affects the middle and end. J Biol Chem. 2020 Dec 11;295(50):17128–37.

63. Doh CY, Kampourakis T, Campbell KS, Stelzer JE. Basic science methods for the characterization of variants of uncertain significance in hypertrophic cardiomyopathy. Front Cardiovasc Med [Internet]. 2023 Aug 1 [cited 2024 Mar 14];10. Available from: https://www.frontiersin.org/articles/10.3389/fcvm.2023.1238515

64. Bers DM. Cardiac excitation–contraction coupling. Nature. 2002 Jan;415(6868):198–205.

65. Spudich JA. The myosin swinging cross-bridge model. Nat Rev Mol Cell Biol. 2001 May;2(5):387–92.

66. Sweeney HL, Houdusse A. Structural and Functional Insights into the Myosin Motor Mechanism. Annu Rev Biophys. 2010 Jun 9;39(Volume 39, 2010):539–57.

67. Villard E, Duboscq-Bidot L, Charron P, Benaiche A, Conraads V, Sylvius N, et al. Mutation screening in dilated cardiomyopathy: prominent role of the beta myosin heavy chain gene. Eur Heart J. 2005 Apr 1;26(8):794–803.

68. Ujfalusi Z, Vera CD, Mijailovich SM, Svicevic M, Yu EC, Kawana M, et al. Dilated Cardiomyopathy Myosin Mutants Have Reduced Force-Generating Capacity. J Biol Chem. 2018 Jun 8;293(23):9017–29.

69. Schmid M, Toepfer CN. Cardiac myosin super relaxation (SRX): a perspective on fundamental biology, human disease and therapeutics. Biol Open. 2021 Feb 15;10(2):bio057646.

70. Marcucci L. Muscle Mechanics and Thick Filament Activation: An Emerging Two-Way Interaction for the Vertebrate Striated Muscle Fine Regulation. Int J Mol Sci. 2023 Jan;24(7):6265.

71. Rasicci DV, Tiwari P, Bodt SM, Desetty R, Sadler FR, Sivaramakrishnan S, et al. Dilated cardiomyopathy mutation E525K in human beta-cardiac myosin stabilizes the interacting-heads motif and super-relaxed state of myosin. Sellers JR, Akhmanova A, Ruppel KM, editors. eLife. 2022 Nov 24;11:e77415.

72. Tobacman LS. Thin Filament-Mediated Regulation of Cardiac Contraction. Annu Rev Physiol. 1996 Mar 1;58(Volume 58, 1996):447–81.

73. Filatov VL, Katrukha AG, Bulargina TV, Gusev NB. Troponin: structure, properties, and mechanism of functioning. Biochem Biokhimiia. 1999 Sep;64(9):969–85.

74. Kobirumaki-Shimozawa F, Inoue T, Shintani SA, Oyama K, Terui T, Minamisawa S, et al. Cardiac thin filament regulation and the Frank–Starling mechanism. J Physiol Sci. 2014 Jul;64(4):221–32.

75. Solaro RJ, Rarick HM. Troponin and Tropomyosin. Circ Res. 1998 Sep 7;83(5):471–80.

76. Galińska-Rakoczy A, Engel P, Xu C, Jung H, Craig R, Tobacman LS, et al. Structural Basis for the Regulation of Muscle Contraction by Troponin and Tropomyosin. J Mol Biol. 2008 Jun 20;379(5):929–35.

77. Sheng JJ, Jin JP. Gene regulation, alternative splicing, and posttranslational modification of troponin subunits in cardiac development and adaptation: a focused review. Front Physiol [Internet]. 2014 Apr 30 [cited 2025 Jun 10];5. Available from: https://www.frontiersin.org/journals/physiology/articles/10.3389/fphys.2014.00165/full

78. Gordon AM, Homsher E, Regnier M. Regulation of Contraction in Striated Muscle. Physiol Rev. 2000 Jan 4;80(2):853–924.

79. Loong CKP, Badr MA, Chase PB. Tropomyosin Flexural Rigidity and Single Ca2+ Regulatory Unit Dynamics: Implications for Cooperative Regulation of Cardiac Muscle Contraction and Cardiomyocyte Hypertrophy. Front Physiol [Internet]. 2012 Apr 4 [cited 2025 Jun 11];3. Available from: https://www.frontiersin.org/journals/physiology/articles/10.3389/fphys.2012.00080/full

80. Risi C, Eisner J, Belknap B, Heeley DH, White HD, Schröder GF, et al. Ca2+-induced movement of tropomyosin on native cardiac thin filaments revealed by cryoelectron microscopy. Proc Natl Acad Sci. 2017 Jun 27;114(26):6782–7.

81. Kelly MA, Caleshu C, Morales A, Buchan J, Wolf Z, Harrison SM, et al. Adaptation and validation of the ACMG/AMP variant classification framework for MYH7-associated inherited cardiomyopathies: recommendations by ClinGen's Inherited Cardiomyopathy Expert Panel. Genet Med Off J Am Coll Med Genet. 2018 Mar;20(3):351–9.

82. Klauke B, Gaertner-Rommel A, Schulz U, Kassner A, Knyphausen E zu, Laser T, et al. High proportion of genetic cases in patients with advanced cardiomyopathy including a novel homozygous Plakophilin 2-gene mutation. PLOS ONE. 2017 Dec 18;12(12):e0189489.

83. Walsh R, Thomson KL, Ware JS, Funke BH, Woodley J, McGuire KJ, et al. Reassessment of Mendelian gene pathogenicity using 7,855 cardiomyopathy cases and 60,706 reference samples. Genet Med. 2017 Feb 1;19(2):192–203.

84. Pugh TJ, Kelly MA, Gowrisankar S, Hynes E, Seidman MA, Baxter SM, et al. The landscape of genetic variation in dilated cardiomyopathy as surveyed by clinical DNA sequencing. Genet Med. 2014 Aug 1;16(8):601–8.

85. Lakdawala NK, Funke BH, Baxter S, Cirino AL, Roberts AE, Judge DP, et al. Genetic Testing for Dilated Cardiomyopathy in Clinical Practice. J Card Fail. 2012 Apr 1;18(4):296–303.

86. Horvat C, Johnson R, Lam L, Munro J, Mazzarotto F, Roberts AM, et al. A gene-centric strategy for identifying disease-causing rare variants in dilated cardiomyopathy. Genet Med. 2019 Jan 1;21(1):133–43.

87. Quiat D, Witkowski L, Zouk H, Daly KP, Roberts AE. Retrospective Analysis of Clinical Genetic Testing in Pediatric Primary Dilated Cardiomyopathy: Testing Outcomes and the Effects of Variant Reclassification. J Am Heart Assoc. 2020 Jun 2;9(11):e016195.

88. Doran MH, Rynkiewicz MJ, Pavadai E, Bodt SML, Rasicci D, Moore JR, et al. Myosin loop-4 is critical for optimal tropomyosin repositioning on actin during muscle activation and relaxation. J Gen Physiol. 2022 Dec 2;155(2):e202213274.

89. Doran MH, Pavadai E, Rynkiewicz MJ, Walklate J, Bullitt E, Moore JR, et al. Cryo-EM and Molecular Docking Shows Myosin Loop 4 Contacts Actin and Tropomyosin on Thin Filaments. Biophys J. 2020 Aug 18;119(4):821–30.

90. Doran MH, Rynkiewicz MJ, Rasicci D, Bodt SML, Barry ME, Bullitt E, et al. Conformational Changes Linked to ADP Release from Human Cardiac Myosin Bound to Actin-Tropomyosin. J Gen Physiol. 2023 Jan 12;155(3):e202213267.

91. Trujillo AS, Hsu KH, Viswanathan MC, Cammarato A, Bernstein SI. The R369 Myosin Residue within Loop 4 Is Critical for Actin Binding and Muscle Function in Drosophila. Int J Mol Sci. 2022 Jan;23(5):2533.

92. Zaru R, Orchard S, Consortium TU. UniProt Tools: BLAST, Align, Peptide Search, and ID Mapping. Curr Protoc. 2023;3(3):e697.

93. Rynkiewicz MJ, Childers MC, Karpicheva OE, Regnier M, Geeves MA, Lehman W. Myosin's powerstroke transitions define atomic scale movement of cardiac thin filament tropomyosin. J Gen Physiol. 2024 Apr 12;156(5):e202413538.

94. Ribeiro AJS, Ang YS, Fu JD, Rivas RN, Mohamed TMA, Higgs GC, et al. Contractility of single cardiomyocytes differentiated from pluripotent stem cells depends on physiological shape and substrate stiffness. Proc Natl Acad Sci U S A. 2015 Oct 13;112(41):12705–10.

95. Ribeiro AJS, Schwab O, Mandegar MA, Ang YS, Conklin BR, Srivastava D, et al. Multi-Imaging Method to Assay the Contractile Mechanical Output of Micropatterned Human iPSC-Derived Cardiac Myocytes. Circ Res. 2017 May 12;120(10):1572–83.

96. Roberts B, Hendershott MC, Arakaki J, Gerbin KA, Malik H, Nelson A, et al. Fluorescent Gene Tagging of Transcriptionally Silent Genes in hiPSCs. Stem Cell Rep. 2019 May 14;12(5):1145–58.

97. Burridge PW, Matsa E, Shukla P, Lin ZC, Churko JM, Ebert AD, et al. Chemically Defined and Small Molecule-Based Generation of Human Cardiomyocytes. Nat Methods. 2014 Aug;11(8):855–60.

98. Lian X, Bao X, Al-Ahmad A, Liu J, Wu Y, Dong W, et al. Efficient Differentiation of Human Pluripotent Stem Cells to Endothelial Progenitors via Small-Molecule Activation of WNT Signaling. Stem Cell Rep. 2014 Nov 11;3(5):804–16.

99. Bremner S, Goldstein AJ, Higashi T, Sniadecki NJ. Engineered Heart Tissues for Contractile, Structural, and Transcriptional Assessment of Human Pluripotent Stem Cell-Derived Cardiomyocytes in a Three-Dimensional, Auxotonic Environment. In: Coulombe KLK, Black III LD, editors. Cardiac Tissue Engineering: Methods and Protocols [Internet]. New York, NY: Springer US; 2022 [cited 2025 Jun 13]. p. 87–97. Available from: https://doi.org/10.1007/978-1-0716-2261-2_6

100. Mohran S, Steczina S, Mandrycky C, Kao K, Regnier M. Measuring the Contractile Kinetics of Isolated Myofibrils from Human-Induced Pluripotent Stem Cell Derived Cardiomyocyte (hiPSC-CM) Models of Cardiomyopathy. In: Regnier M, Childers M, editors. Familial Cardiomyopathies [Internet]. New York, NY: Springer US; 2024 [cited 2025 Jun 12]. p. 213–33. (Methods in Molecular Biology; vol. 2735). Available from: https://link.springer.com/10.1007/978-1-0716-3527-8_12

101. Brooks D, Bawa S, Bontrager A, Stetsiv M, Guo Y, Geisbrecht ER. Independent pathways control muscle tissue size and sarcomere remodeling. Dev Biol. 2022 Oct;490:1–12.

102. Duong H, Wu B, Tawil B. Modulation of 3D Fibrin Matrix Stiffness by Intrinsic Fibrinogen–Thrombin Compositions and by Extrinsic Cellular Activity. Tissue Eng Part A. 2009 Jul;15(7):1865–76.

103. Marchianò S, Bertero A, Murry CE. Learn from Your Elders: Developmental Biology Lessons to Guide Maturation of Stem Cell-Derived Cardiomyocytes. Pediatr Cardiol. 2019 Oct 1;40(7):1367–87.

104. Ribeiro AJS, Ang YS, Fu JD, Rivas RN, Mohamed TMA, Higgs GC, et al. Contractility of Single Cardiomyocytes Differentiated from Pluripotent Stem Cells Depends on Physiological Shape and Substrate Stiffness. Proc Natl Acad Sci. 2015 Oct 13;112(41):12705–10.

105. Pioner JM, Racca AW, Klaiman JM, Yang KC, Guan X, Pabon L, et al. Isolation and Mechanical Measurements of Myofibrils from Human Induced Pluripotent Stem Cell-Derived Cardiomyocytes. Stem Cell Rep. 2016 May 5;6(6):885–96.

106. Lee S, Vander Roest AS, Blair CA, Kao K, Bremner SB, Childers MC, et al. Incomplete-penetrant hypertrophic cardiomyopathy MYH7 G256E mutation causes hypercontractility and elevated mitochondrial respiration. Proc Natl Acad Sci. 2024 May 7;121(19):e2318413121.

107. Steczina S, Mohran S, Bailey LRJ, McMillen TS, Kooiker KB, Wood NB, et al. MYBPC3-c.772G>A mutation results in haploinsufficiency and altered myosin cycling kinetics in a patient induced stem cell derived cardiomyocyte model of hypertrophic cardiomyopathy. J Mol Cell Cardiol. 2024 Jun 1;191:27–39.

108. Planelles-Herrero VJ, Hartman JJ, Robert-Paganin J, Malik FI, Houdusse A. Mechanistic and Structural Basis for Activation of Cardiac Myosin Force Production by Omecamtiv Mecarbil. Nat Commun. 2017 Aug 4;8(1):190.

109. Childers MC, Regnier M. Dynamics of the Pre-Powerstroke Myosin Lever Arm and the Effects of Omecamtiv Mecarbil. Int J Mol Sci. 2024 Jan;25(19):10425.

110. Webb B, Sali A. Comparative Protein Structure Modeling Using MODELLER. Curr Protoc Protein Sci. 2016 Nov 1;86:2.9.1-2.9.37.

111. Case DA, Aktulga HM, Belfon K, Cerutti DS, Cisneros GA, Cruzeiro VWD, et al. AmberTools. J Chem Inf Model. 2023 Oct 8;63(20):6183–91.

112. Li P, Merz KM. Taking into Account the Ion-induced Dipole Interaction in the Nonbonded Model of Ions. J Chem Theory Comput. 2014 Jan 14;10(1):289–97.

113. Li P, Song LF, Merz KMJr. Parameterization of Highly Charged Metal Ions Using the 12-6-4 LJ-Type Nonbonded Model in Explicit Water. J Phys Chem B. 2015 Jan 22;119(3):883–95.

114. Li P, Song LF, Merz KMJr. Systematic Parameterization of Monovalent Ions Employing the Nonbonded Model. J Chem Theory Comput. 2015 Apr 14;11(4):1645–57.

115. Jorgensen WL, Chandrasekhar J, Madura JD, Impey RW, Klein ML. Comparison of simple potential functions for simulating liquid water. J Chem Phys. 1983 Jul 15;79(2):926–35.

116. Maier JA, Martinez C, Kasavajhala K, Wickstrom L, Hauser KE, Simmerling C. ff14SB: Improving the Accuracy of Protein Side Chain and Backbone Parameters from ff99SB. J Chem Theory Comput. 2015 Aug 11;11(8):3696–713.

117. Kiani FA, Fischer S. Catalytic strategy used by the myosin motor to hydrolyze ATP. Proc Natl Acad Sci. 2014 Jul 22;111(29):E2947–56.

118. He X, Man VH, Yang W, Lee TS, Wang J. A fast and high-quality charge model for the next generation general AMBER force field. J Chem Phys. 2020 Sep 16;153(11):114502.

119. Roe DR, Cheatham TEI. PTRAJ and CPPTRAJ: Software for Processing and Analysis of Molecular Dynamics Trajectory Data. J Chem Theory Comput. 2013 Jul 9;9(7):3084–95.

120. Lehman W, Karpicheva OE, Rynkiewicz MJ. BPS2025 - Tropomyosin snapback on actin after myosin detachment from cardiac thin filaments. Biophys J. 2025 Feb 13;124(3):613a–4a.

121. Risi C, Schäfer LU, Belknap B, Pepper I, White HD, Schröder GF, et al. High-Resolution Cryo-EM Structure of the Cardiac Actomyosin Complex. Structure. 2021 Jan 7;29(1):50-60.e4.

122. Kao K, Geeves MA. Protocols for Myosin and Actin-Myosin Assays Using Rapid, Stopped-Flow Kinetics. In: Regnier M, Childers M, editors. Familial Cardiomyopathies: Methods and Protocols [Internet]. New York, NY: Springer US; 2024 [cited 2025 Jun 13]. p. 191–211. Available from: https://doi.org/10.1007/978-1-0716-3527-8_11

123. Iorga B, Schwanke K, Weber N, Wendland M, Greten S, Piep B, et al. Differences in Contractile Function of Myofibrils within Human Embryonic Stem Cell-Derived Cardiomyocytes vs. Adult Ventricular Myofibrils Are Related to Distinct Sarcomeric Protein Isoforms. Front Physiol [Internet]. 2018 Jan 19 [cited 2025 Jun 13];8. Available from: https://www.frontiersin.org/journals/physiology/articles/10.3389/fphys.2017.01111/full

124. van der Velden J, Stienen GJM. Cardiac Disorders and Pathophysiology of Sarcomeric Proteins. Physiol Rev. 2019 Jan;99(1):381–426.